Original Paper

Assessment of Thermal Maturity, Source Rock Potential and Paleodepositional Environment of the Paleogene Lignites in Barsingsar, Bikaner–Nagaur Basin, Western Rajasthan, India

Alok K. Singh[1,2] and Alok Kumar[1]

Investigations on the Paleogene lignites were carried out through geochemical, mineralogical and petrographic analyses to assess their paleodepositional environment, source rock potential and thermal maturity. The samples were collected from the Barsingsar lignite mines in the Bikaner–Nagaur Basin, Western Rajasthan, India. Huminite reflectance assigns these samples as lignite (low-rank coal). Barsingsar lignites are dominated by the huminite maceral group, while inertinites and liptinites occur in subordinated amount. The mineral matter is dominated by carbonates, pyrite and argillaceous (in descending order). Gelification index, tissue preservation index, groundwater index and vegetation index indicate the prevalence of a dry forest swamp having ombrotrophic to mesotrophic conditions in the paleomire. Rock–Eval pyrolysis indicates high hydrogen index relative to oxygen index and excellent hydrocarbon potential. The Barsingsar lignites are characterized by mixed type III and type II kerogens, which are thermally immature. Several minerals like quartz, coesite, siderite, aragonite and rutile minerals have been identified by XRD analysis, whereas selected trace elements primarily Sr, Zr, Cu, Pb, Zn, Cr, V, Ni, Rb and Co were also detected. Fourier-transform infrared spectroscopy pattern shows the dominance of clay minerals and the presence of aromatic, aliphatic and some oxygen functional groups in these lignites.

INTRODUCTION

Coal and lignite are major primary sources of energy in many countries. Due to continued increase in the price of high-rank coals, attention is being given to low-rank coal as an important sustainable energy resource. Therefore, researchers are making serious efforts to understand the characteristics of low-rank coals, especially lignites, for their optimum utilization (Fowler et al. 1991; Bechtel et al. 2007a, b; Koukouzas et al. 2010; Dutta et al. 2011; Singh et al. 2013, 2016a, 2017a, 2018; Ayinla et al. 2017a; Ðoković et al. 2017; Karayiğit et al. 2017; Radhwani et al. 2018).

Huge lignite resources occur in few European countries, Australia, Nigeria as well as in some developing countries of Asia (Singh and Kumar 2017a). There are reports on hydrocarbon-prone lignite in Poland (Bechtel et al. 2007a), Austria

[1]Department of Petroleum Engineering and Geological Science, Rajiv Gandhi Institute of Petroleum Technology, Jais, Amethi 229304, India.

[2]To whom correspondence should be addressed; e-mail: asingh@rgipt.ac.in; drsinghalokk@gmail.com

(Bechtel et al. 2007b), Tunisia (Radhwani et al. 2018), Serbia (Đoković et al. 2017), Turkey (Karayiğit et al. 2017), Nigeria (Ayinla et al. 2017a), India (Dutta et al. 2011; Singh 2012; Singh et al. 2016a, b, 2017a, 2018), Greece (Fowler et al. 1991; Koukouzas et al. 2010) and Pakistan (Ahmad et al. 2015). In India, lignite is found in the Western Rajasthan, Tamil Nadu, Gujarat and Jammu and Kashmir states (Singh et al. 2010, Prasad et al. 2009).

During Jurassic and Cretaceous Periods, due to the global tectonic process, the Indian plate got separated from Gondwana. Subsequently, development of rift basin took place in the Western Rajasthan, which represents the Phanerozoic geologic evolution of the area (Shivanna and Singh 2016). Jaisalmer Basin, Bikaner–Nagaur Basin and Barmer–Sanchore Basin were developed during the Phanerozoic crustal evolution of Western Rajasthan (Bhandari 1999) (Fig. 1a). The shallow marine sediment succession and sand-covered area of Palana and Merta sub-basins in Bikaner and Nagaur districts are of Lower Tertiary (Pareek 1981, 1984; Shivanna and Singh 2016). Over the last few decades, these sedimentary deposits have got great attention in view of encouraging prospects of various mineral deposits and for the study of paleoenvironmental condition of the region. In relevance to source rock characterization, paleoenvironmental condition, palynology and minerals in lignites of these basins, valuable contributions have been made by Mukherjee et al. (1992), Tripathi et al. (2009), Singh et al. (2012), Raju and Mathur (2013), Shukla et al. (2014), Bhattacharya and Dutta (2015), Farrimond et al. (2015), Singh et al. (2015), Kumar et al. (2016), Paul and Dutta (2016), Shivanna and Singh (2016), Shivanna et al. (2016), Singh et al. (2015, 2016a, b, 2017a, b, 2018), Singh and Kumar (2017a, b, 2018a, b). The present research work aims to study the paleoenvironmental condition, source rock characteristics and mineralogy of lignite deposits of Barsingsar, Bikaner–Nagaur Basin, which is a relatively less studied region.

GEOLOGICAL SETTING AND LITHOLOGY OF THE STUDY AREA

Various sedimentary basins have been identified in Western Rajasthan. These basins are bounded between the Aravalli and Delhi Supergroup rocks as easternmost boundary and the Malani Igneous suite as the southern boundary (Fig. 1a) (Pa-

reek 1981; Roy and Jakhar 2002). These basins include Marwar Basin (Cambrian), Bap-Badhura remnant (Permian), Lathi Basin (Lower Jurassic), Jaisalmer Basin (Mesozoic and Tertiary), Palana-Ganganagar Shelf (Tertiary) and Barmer Basin (Cretaceous to Tertiary) (Pareek 1981). Outcrops of different ages occur in the Bikaner district. Bilara group is composed of dolomite and limestone and shows algal structure. The Nagaur Group rocks are comprised of siltstone containing gypsum and clay pockets along with sandstone. The Bap Boulder Bed (Permo-Carboniferous) overlies the Marwar Supergroup. It consists of glacial drift deposits such as boulders, cobbles and erratic rocks of the Malani Igneous Suite, Delhi Supergroup and Marwar Supergroup. The Palana Formation occurs above the Bap Boulder Bed, contains shale, clay and lignite seams. The Palana Formation is succeeded by the Marth and Jogira Formations. The uppermost section of the area is represented by Quaternary sediments of varying thickness (Fig. 1a).

The entire investigation area is covered by eolians with thickness varying from 1.5 to 4.0 m. Eolian sand is underlain by white to yellowish white calcareous *kankar* column. This horizon is underlain by medium to coarse-grained buff-colored sandstone, followed by variegated clay. Variegated clay acts as the roof of the lignite and carbonaceous horizon (Fig. 1b).

METHOD OF STUDY

Sixty samples were collected from the working face of the Barsingsar mine, Bikaner–Nagaur Basin following pillar sampling method from bottom to top to cover the entire thickness of the seam. The reported thickness of seam is about 43 m, but outcrop does not show actual thickness. The ICCP (1993) scheme has been used for megascopic characterization. The samples with similar megascopic properties were clubbed together and converted into a single composite band for the petrographic and geochemical studies.

Petrographic Analysis

Thirteen composite samples were taken for petrographic analysis. The lignite samples were crushed into − 18 mesh size, dried and molded using epoxy resin to prepare the polished particulate
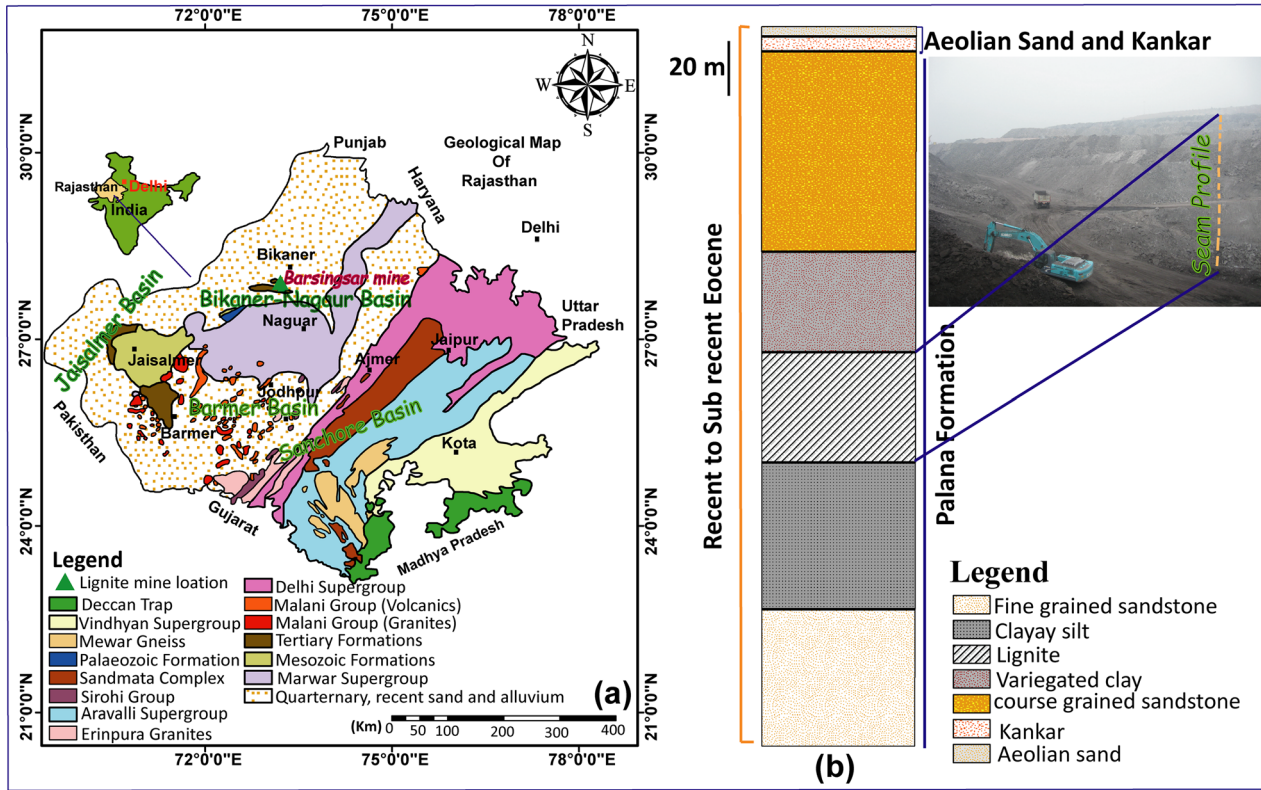
Figure 1. **a** Geological map of Rajasthan showing location of Barsingsar lignite mine, Bikaner–Nagaur Basin, India, **b** generalized lithostratigraphic sequence of Barsingsar block.

mounts for microscopic study following the ASTM Standard D7708-11 (2011). An advanced petrological microscope (Leica DM 2700P), with reflected and fluorescence light facilities attached with the MSP 200 photometric system for reflectance measurement, has been used for petrographic study. The petrographic analysis was carried out in concurrence with the guidelines established by the International Committee for Coal and Organic Petrology, ICCP-94 system (ICCP 2001, 2005, 2017). More than 500 maceral points were counted on each polished pellet using a PetrogLite point counter machine during petrographic analysis. More than 100 random reflectance measurements were performed on the scratch-free eu-ulminite-B maceral as per the ISO norms (ISO 7404-5 2009) on each polished block.

The key information about the coal facies and paleodepositional environment condition during peat accumulation of the area was identified from petrographic indices derived from macerals ratios (Baboolal et al. 2016; Oskay et al. 2016). Indices, such as TPI (tissue preservation index), GWI

(groundwater index), VI (vegetation index) and GI (gelification index), have been proposed by Diessel (1986) and Calder et al. (1991) for Permian coal, and further modified by Bechtel et al. (2003) and Kalkreuth et al. (1991) for Paleogene coals. For the calculation of GWI, ash content has been used because it provides better and precise quantitative information about the mineral content than the mineral matter analyzed under microscope (Stock et al. 2016). The TPI vs. GI and GWI vs. VI plots were used to assess peat-forming conditions and predominant peat-forming vegetation. GI is derived from the ratio of gelinite and fusinitized maceral, and it gives an idea about the availability of water during peat formation. TPI can be defined as the ratio of structural tissues vs. destructed tissues, and it delivers evidence about the degree of humification and vegetation type. GWI is the ratio of strongly gelified to weakly gelified tissue and provides information about the hydrogeological condition. VI can be used to indicate the type of vegetation (Calder et al. 1991). The following formulae were used:

$$GI = \frac{\text{texto ulminite} + \text{eu} - \text{ulminite} + \text{corpohuminite} + \text{densinite} + \text{macrinite}}{\text{textinite} + \text{attrinite} + \text{fusinite} + \text{inertodetrinite}},$$

$$TPI = \frac{\text{textinite} + \text{textoulmiite} + \text{eu} - \text{ulminite} + \text{corpohuminite} + \text{fusinite}}{\text{attrinite} + \text{densinite} + \text{macrinite}},$$

$$VI = \frac{\text{telohuminite} + \text{fusinite} + \text{semifusinite} + \text{suberinite} + \text{resinite}}{\text{dt.huminite} + \text{inertodetrinite} + \text{liptodetrinite} + \text{alginite} + \text{sporinite} + \text{cutinite}} \text{ and}$$

$$GWI = \frac{\text{gelinite} + (\text{ash ontent}/2)}{\text{textinite} + \text{ulminite} + \text{corpohuminite}}$$

Facies diagram given by Mukhopadhyay (1989) has been used to establish the paleomire and prevalent oxygen conditions.

Geochemical Analysis

To determine the weight percent of fixed carbon, ash, volatile matter and moisture (proximate analysis), the guidelines of BIS (2003) were used. For each entity, 1 g of powdered (− 72 mesh) sample was taken. The moisture content was determined at a temperature of 105 °C for 1 h in a hot air oven. The powdered sample was heated at a temperature of 450 °C and 750 ± 25 °C for about half an hour and 1 h, respectively, in a muffle furnace to determine the ash content. The volatile matter was determined by keeping the samples at temperature 925 °C for exactly 7 min in the furnace. The value of fixed carbon (in percent) was obtained by subtracting ash, moisture and volatile matter from hundred. As part of the investigation, an ultimate analysis was performed to determine the carbon, hydrogen, nitrogen, sulfur and oxygen content as per the guidelines of ASTM D5373-08 (1993).

The pyrolysis was performed on Rock–Eval 6 analyzer. The samples were pyrolyzed in an inert atmosphere, and the remaining carbon was consecutively cooked in an oxidation oven. The hydrocarbons released were detected by a flame ionization detector throughout pyrolysis. The released CO and CO_2 were monitored continuously using online infrared detectors. The samples were first pyrolyzed from 300 to 650 °C at a rate of 25 °C/min. At a temperature of 300 °C, the oxidation phase was started with an isothermal stage. After that, the temperature was increased to 750 °C at a rate of 25 °C/min to burn out all the residual carbon.

Mineralogical Analysis

To study the mineralogy of the Barsingsar lignite, the samples were subjected to XRD (X-ray diffrac-

tion), XRF (X-ray fluorescence) and FT-IR (Fourier-transform infrared spectroscopy) analysis. The XRD analysis was conducted on the ash of three composite lignite samples from top, middle and bottom of the exposed section using Panalytica XRD for ultra-fast X-ray diffraction on powder samples using the line detector. The measurement was taken within the angle range of 10–75° 2θ. X'pert HighScore software was used for identification of mineral present in the analyzed sample. To determine the concentration of major oxides and trace elements, XRF analysis was performed on pressed ash of lignite powder pellets using Rigaku-made WD-XRF Machine. FT-IR spectra were recorded in FT-IR spectrophotometer on powdered lignite samples using ATR mode. A spectral resolution of 4 cm^{-1} at a range of 400–4000 cm^{-1} was used in collecting IR spectra.

RESULTS AND DISCUSSION

Macroscopic Observations

Brown coal is normally categorized into four main lithotypes: matrix rich, xylite rich, charcoal rich and mineral rich (ICCP 1993; Taylor et al. 1998). Matrix-rich lithotype consists of fine detrital humic groundmass with homogeneous appearance (Thomas 2002). Xylite-rich lithotype comprises well-fossilized wood fragments. Charcoal-rich lithotype is observed as coke-like appearances mainly found as a lens. Mineral-rich lithotype is identified as different kinds of mineral association with high specific gravity (Thomas 2002).

Macroscopically, the analyzed lignite samples are dark brown to black in color, containing sometimes resin grains and wood fragments. Matrix-rich lignite is the most common lithotype along with the xylite-rich, while charcoal-rich and mineral-rich lithotypes were absent in the Barsingsar (Fig. 2). The roof and floor of the lignite seam are clay and clayey silt, respectively.
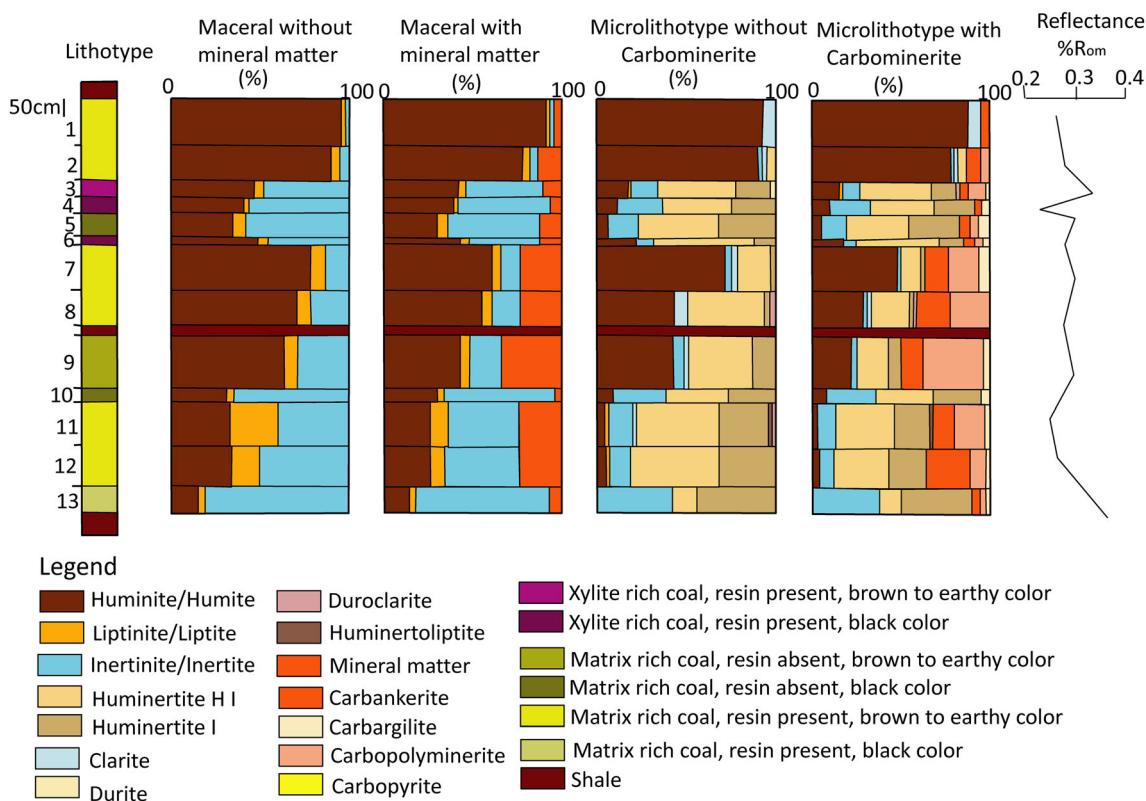
Figure 2. Graphic representation showing the variation in lithotype, maceral and microlithotype with mineral matter and mineral matter-free basis and mean huminite/vitrinite reflectance of Barsingsar lignite, Rajasthan, India.

Microscopic Observations

The graphical representation of the variation of lithotype, maceral, microlithotype and mean huminite reflectance is shown in Figure 2. Petrographic constituents of low-rank coals were identified based on their different morphological characteristics and color under reflected as well as fluorescent light (Teichmüller 1974; Hasiah 1999; Abdullah 2003; Hakimi et al. 2013; ICCP 2017). The Barsingsar lignite samples are dominated by huminite macerals (13.7–91.5 vol% with mean 44.3 vol%) followed by inertinite (1.9–76.0 vol% with mean 35.4 vol%). Liptinite is less abundant in these lignites (2.2–9.5 vol% with mean 4.9 vol%). Mineral matter occurs in significant amount (3.8–33.6 vol% with mean 15.4 vol%) and is dominated by carbonates, whereas clay and pyrites occur in meager concentrations (Table 1). Random mean huminite reflectance (%R_{om}) values of Barsingsar samples are given in Table 2. The %R_{om} values lie between 0.22 and 0.36% indicating low-rank (lignite) stage.

Huminite group is mainly represented by attrinite corpohuminite and textinite. Textinite macerals are gray in color showing ungelified cell wall structure. The cell lumens of textinite are mostly filled with corpohuminite, carbonate and clay minerals (Fig. 3a). The textinite is derived from plants, both herbaceous and arborescent with woody tissues. A notable concentration of textinite maceral indicates cell tissue preservation under relatively dry forest (Diessel 1992). Clusters of phlobaphinite/corpohuminite on the patch of attrinite and attrinite are associated with carbonate minerals (Fig. 3b). Attrinite consists of fine-grained humic particles of different shapes, spongy to porous in nature and light to dark gray in color. The concentration of gelified ulminite maceral is less than ungelified textinite. Minor concentration of gelinite was recorded in the Barsingsar lignite, in which porigelinite appears as spongy, porous and micro-granular showing brownish color and associated with corpohuminite (Fig. 3c).

Liptinite macerals are low in concentration and are mainly represented by sporinite and resinite,

Table 1. Frequency distribution of maceral and mineral matter composition (in volume percent) under white incident light and blue irradiation in lignites of Barsingsar, Bikaner, Rajasthan

S. no.	Coalfield	Coal seam	Band no.	Huminite								
				Textinite	Ulminite	Gelinite	Carpo huminite	Atrinite	Densinite	Porigelinite	Detrohuminite	Phloba phinite
			Bottom									
1	Barsingsar	BS	1	7.91	7.67	2.72	32.11	31.99	1.53	0.47	0.83	6.26
2	Barsingsar	BS	2	9.61	7.38	4.74	13.23	33.71	0.14	2.65	0.84	5.43
3	Barsingsar	BS	3	3.75	8.19	1.25	6.11	20.14	0.28	0.69	1.39	0.28
4	Barsingsar	BS	4	4.92	8.20	1.94	5.51	14.01	0.45	0.45	2.38	0.75
5	Barsingsar	BS	5	1.24	7.45	Nil	5.72	13.29	Nil	Nil	2.63	Nil
6	Barsingsar	BS	6	3.86	5.50	Nil	14.54	14.99	0.89	0.30	2.23	0.59
7	Barsingsar	BS	7	9.66	8.41	Nil	22.74	16.05	0.47	0.78	1.87	1.09
8	Barsingsar	BS	8	9.44	6.82	0.13	8.65	23.19	0.52	0.66	4.33	0.79
9	Barsingsar	BS	9	5.39	4.70	0.83	11.88	16.02	1.24	Nil	1.80	0.69
10	Barsingsar	BS	10	2.90	5.43	0.72	7.07	11.77	0.18	0.18	1.63	Nil
11	Barsingsar	BS	11	2.95	0.31	Nil	3.27	16.98	0.31	Nil	1.56	0.16
12	Barsingsar	BS	12	1.35	1.20	0.15	2.56	16.84	1.65	Nil	2.11	Nil
13	Barsingsar	BS	13	0.35	0.52	Nil	1.38	10.89	Nil	Nil	0.52	Nil
			Top									
			Mean	4.87	5.52	1.56	10.37	18.45	0.70	0.77	1.86	1.78

S. no.	Coalfield	Coal seam	Band no.	Liptinite							
				Sporinite	Cutinite	Resinite	Suberinite	Alginite	Bituminite	Liptodetrinite	Fluorinite
			Bottom								
1	Barsingsar	BS	1	0.35	Nil	0.24	1.65	Nil	Nil	Nil	Nil
2	Barsingsar	BS	2	0.70	0.56	1.25	0.84	Nil	Nil	0.42	Nil
3	Barsingsar	BS	3	0.56	0.14	2.78	Nil	Nil	Nil	0.83	Nil
4	Barsingsar	BS	4	1.19	Nil	0.75	Nil	Nil	Nil	0.30	Nil
5	Barsingsar	BS	5	2.32	0.46	1.39	Nil	Nil	Nil	1.70	Nil
6	Barsingsar	BS	6	1.48	2.37	0.45	0.62	Nil	Nil	0.45	Nil
7	Barsingsar	BS	7	3.12	0.62	0.93	0.13	Nil	Nil	0.16	Nil
8	Barsingsar	BS	8	0.66	Nil	4.46	Nil	Nil	Nil	0.79	Nil
9	Barsingsar	BS	9	1.93	0.55	1.52	Nil	Nil	Nil	0.41	Nil
10	Barsingsar	BS	10	2.36	Nil	0.54	0.16	Nil	Nil	0.54	Nil
11	Barsingsar	BS	11	2.02	0.31	6.23	Nil	Nil	Nil	0.78	Nil
12	Barsingsar	BS	12	1.80	0.15	5.56	Nil	Nil	Nil	0.45	Nil
13	Barsingsar	BS	13	2.25	0.52	0.52	Nil	Nil	Nil	0.35	Nil
			Top								
			Mean	1.60	0.63	2.05	0.68			0.60	

Table 1. continued

S. no.	Coalfield	Coal seam	Band no.	Inertinite						Mineral matter		
				Semifusinite	Fusinite	Macrinite	Micrinite	Funginite	Inertodetrinite	Sulfide	Carbonate	Argillaceous
			Bottom									
1	Barsingsar	BS	1	0.47	0.12	Nil	Nil	1.30	Nil	0.24	4.13	0.35
2	Barsingsar	BS	2	2.92	0.70	Nil	Nil	0.84	Nil	0.42	13.09	0.56
3	Barsingsar	BS	3	22.08	10.56	0.69	0.69	2.78	5.97	0.56	7.50	2.78
4	Barsingsar	BS	4	22.50	21.31	0.30	0.75	1.94	6.71	0.30	1.49	3.87
5	Barsingsar	BS	5	29.21	9.58	2.16	0.31	2.01	7.26	0.31	7.88	5.10
6	Barsingsar	BS	6	24.48	6.68	0.30	0.59	2.67	5.04	0.45	8.61	3.56
7	Barsingsar	BS	7	4.05	3.27	Nil	Nil	0.93	2.34	2.65	17.45	2.80
8	Barsingsar	BS	8	6.42	1.70	0.13	Nil	2.36	4.98	4.33	18.61	0.92
9	Barsingsar	BS	9	9.67	2.62	0.55	Nil	2.49	4.14	9.12	21.27	3.18
10	Barsingsar	BS	10	32.97	19.20	1.63	0.36	1.81	6.88	0.18	1.09	2.54
11	Barsingsar	BS	11	16.98	2.34	1.40	0.31	10.75	9.66	8.26	13.86	1.40
12	Barsingsar	BS	12	24.36	5.26	0.45	0.45	1.20	10.23	3.01	20.15	1.05
13	Barsingsar	BS	13 Top	61.31	6.74	0.35	0.17	0.17	7.25	0.86	3.45	2.42
			Mean	19.80	6.93	0.80	0.45	2.40	6.41	2.36	10.66	2.35

whereas suberinite, cutinite and liptodetrinite occur sparsely. Resinite is mainly associated with humotelinite and humodetrinites. It also occupies cell lumens as a lumpy body, and it has orange to dark orange color in reflected white light (Fig. 3d), while in fluorescent blue light, it looks pale brownish yellow color. Suberinite was recorded in minor concentration, appearing dark in color under reflected white light (Fig. 3e). Sporinites consist of outer membranes termed as exines and perines of spore and pollens. Sporangium is observed under UV light in a few samples (Fig. 3f).

Fusinite, semifusinite, funginite and inertodetrinite occur as predominant sub-macerals of the inertinite group. Semifusinite shows intermediate reflectance between huminite and fusinite. The tissue structures vary in size and are smaller than fusinite (Fig. 3g). Fusinite displays very high reflectance with well-preserved cellular structure (Fig. 3h). The cluster of single-celled, rounded funginite appears in the groundmass of ulminite maceral (Fig. 3g). Few tiny patches of inertodetrinite with high reflectance were also observed in the studied samples (Fig. 3g). In addition, some massive, dispersed, cell fillings and disseminated patches of carbonate, sulfide and clay minerals were also recorded in the Barsingsar lignites (Fig. 3a–e and i).

Coal Rank

The huminite reflectance has been a widely used parameter for rank determination along with proximate analysis data, such as moisture and calorific value (O'Keefe et al. 2013). The low huminite reflectance (0.22–$0.36\% R_{om}$) in study area put these coals as low rank (lignite) (Table 2). This could be due to the presence of hydrogen-rich macerals (e.g., liptinite group) (Bechtel et al. 2016). The high concentration of huminite with low liptinite content reported in Barsingsar supports the hypothesis that these lignites are of humic type in nature.

Coal Facies and Paleodepositional Environment

Petrographic constituents of coals have been widely used to infer the depositional environment of the paleomires (i.e., Baboolal et al. 2016; Ayinla et al. 2017b; Johnston et al. 2017; Singh and Kumar 2017b; Singh et al. 2017b, c; Guo et al. 2018). The

Table 2. Result of reflectance measurement and petrographic indices of lignites of Bikaner basin (Barsingsar lignite mines)

S. no.	Coalfield	Coal seam	Band no.	Ro min%	Ro mean%	Ro max%	GI	TPI	GWI	VI
			Bottom							
1	Barsingsar	BS	1	0.22	0.26	0.36	1.23	1.43	3.24	15.31
2	Barsingsar	BS	2	0.24	0.28	0.37	0.69	0.91	7.58	9.01
3	Barsingsar	BS	3	0.25	0.34	0.43	0.47	1.36	2.21	5.33
4	Barsingsar	BS	4	0.20	0.22	0.24	0.42	2.72	2.71	5.45
5	Barsingsar	BS	5	0.26	0.30	0.35	0.53	1.55	0.71	3.40
6	Barsingsar	BS	6	0.23	0.28	0.38	0.82	1.89	0.57	3.54
7	Barsingsar	BS	7	0.21	0.27	0.36	1.32	2.67	1.02	3.32
8	Barsingsar	BS	8	0.22	0.30	0.42	0.65	1.12	1.16	2.69
9	Barsingsar	BS	9	0.21	0.27	0.36	0.84	1.38	1.59	2.71
10	Barsingsar	BS	10	0.22	0.30	0.45	0.42	2.55	1.29	5.35
11	Barsingsar	BS	11	0.22	0.25	0.28	0.21	0.93	2.17	2.02
12	Barsingsar	BS	12	0.21	0.26	0.31	0.21	0.55	3.62	2.56
13	Barsingsar	BS	13	0.26	0.36	0.49	0.10	0.80	5.13	6.38
			Top							

GI gelification index, *TPI* tissue preservation index, *GWI* groundwater index, *VI* vegetation index, %R_{om} mean huminite reflectance
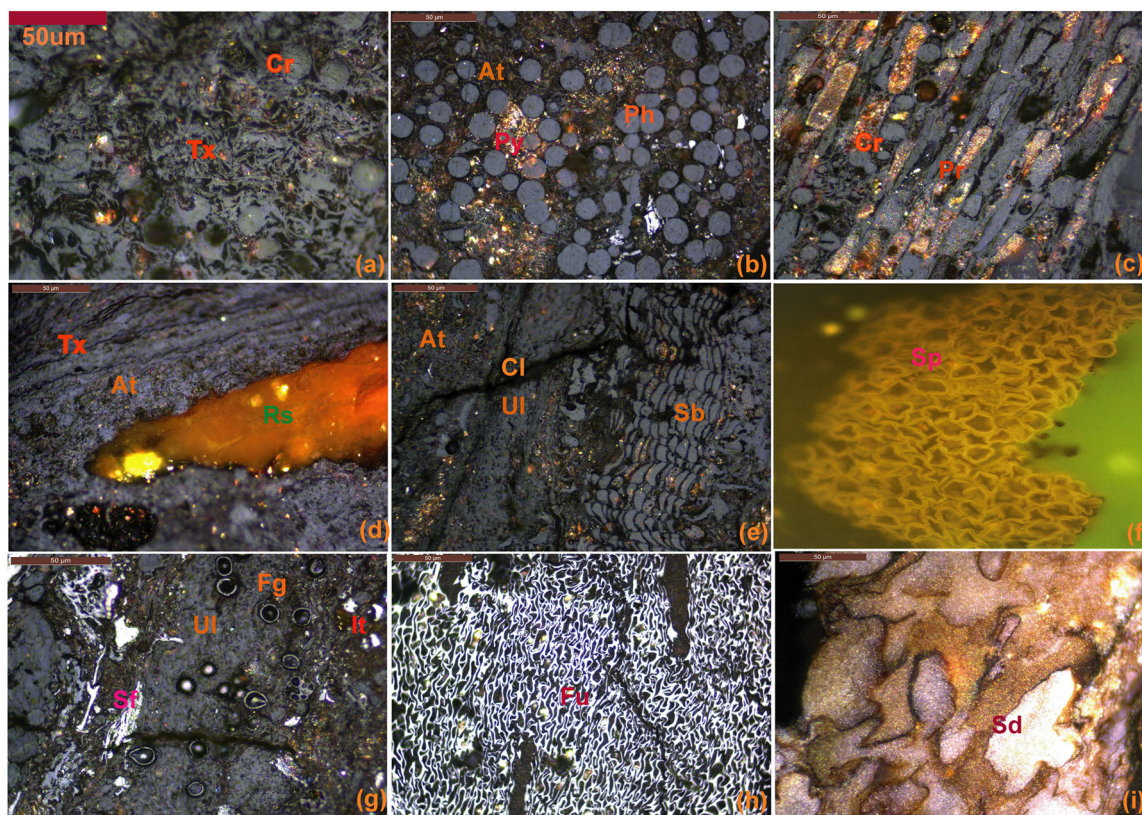

Plate:(a) Textinite with corpohuminite; (b) Phlobaphinite in attrinite associated with pyrite; (c) Porigelinite; (d) Resinite;
(e) Suberinite & ulminite; (f) sporinites; (g) Funginite & semifusinite; (h) Fusinite; (i) Siderite
[Tx=textinite; Cr=Corpohuminite; At=Attrinite; Ph=Phlobaphinite; Pr=Porigelinite; Py=Pyrite; Rs=Resinite; Ul=Ulminite; Cl=Clay;
Sp=Sporinite; Fg=Funginite; Sf=Semifusinite; It=Inertodetrinite; Fu=Fusinite; Sd=Siderite

Figure 3. Representative photomicrographs of macerals and mineral matter of Barsingsar lignites, under the white light as well as UV light.
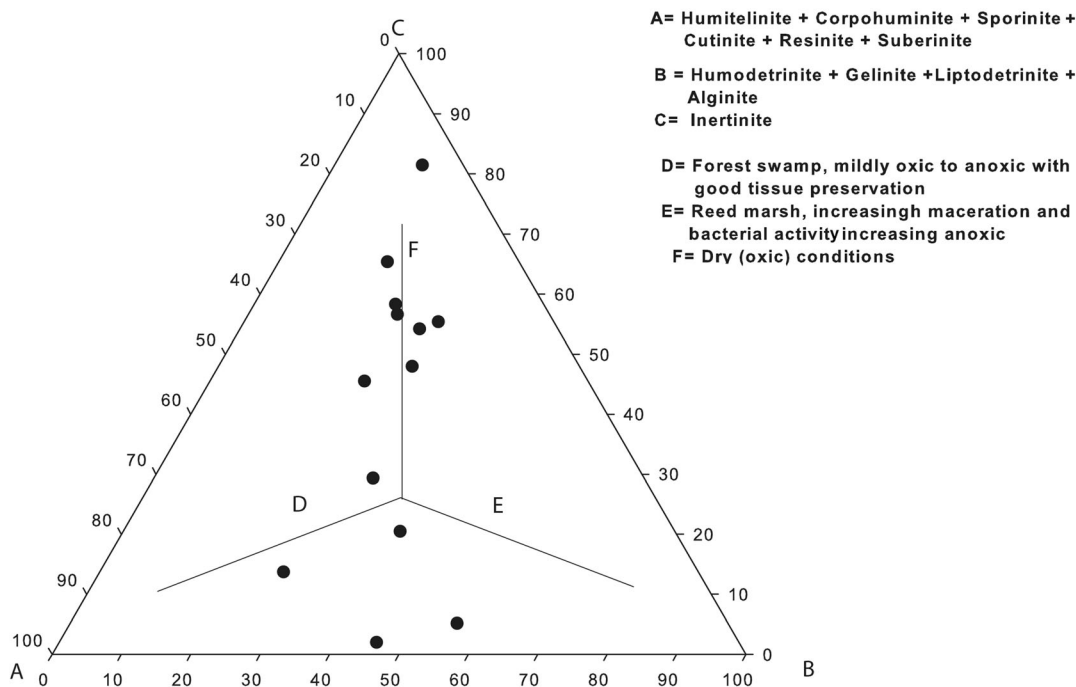
Figure 4. Facies diagram showing peat-forming conditions in the study area (modified from Mukhopadhyay 1986).

higher concentration of huminite (Table 1), especially detrohuminite, in the Barsingsar lignite sample indicates abundance of herbaceous plant community. The moderate to high concentrations of inertinite, intermittently, suggests prevalence of oxidation condition in the paleomire, which resulted in charring effect leading to the formation of more amounts of inertinite macerals. In addition, the studied lignite samples show significant amount of ulminite and porigelinites, which entails preservation of more plant tissues that compressed and gelified under wet conditions (Diessel 1992; Sykorova et al. 2005).

In the ternary diagram (Fig. 4), sample points mostly fall near the vertex C and a few are between vertices A and B (Mukhopadhyay 1989). The samples follow this trend due to higher inertinite contents. The sample points, which mostly fall in the F field in the ternary diagram, suggest dry (oxic) conditions during peat accumulation (Fig. 4). All the Barsingsar lignite samples have shown low and variable TPI (0.55–2.72) and GI (0.10–1.32) values, which suggest predominance of herbaceous plants in the mire and low to moderate preservation of organic matter (Diessel 1992; Oskay et al. 2016). This can be supported by the very low concentration of

liptinite maceral with the presence of detrital of semifusinite and fusinite (inertodetrinite) in the study area. The coal facies diagram for the Barsingsar lignite (Fig. 5a) indicates that these coals have originated under a dry forest swamp condition. The plot of the coal facies of Barsingsar lignites based on GWI (0.57–7.58) and VI (2.02–15.31), as shown in Figure 5b, indicates that these lignites originated from bog forest and ombrotrophic to mesotrophic hydrological condition in the area.

In addition, according to Chou (2012), sulfur in low sulfur coals ($< 1\%$ S) is derived from plant material and related to fluvial environments, whereas medium (1 to $< 3\%$ S) and high ($\geq 3\%$ S) sulfur coals indicate sulfate in seawater that flooded the peat swamp and are related to seawater-influenced environment. The low sulfur (0.18–0.97%) recorded in Barsingsar area indicates that the sulfur was derived from plant material and shows the influence of fluvial environments in the region.

Ultimate and Proximate Analyses

Summaries of the outcomes of the ultimate and proximate analyses of lignite samples of the Bars-
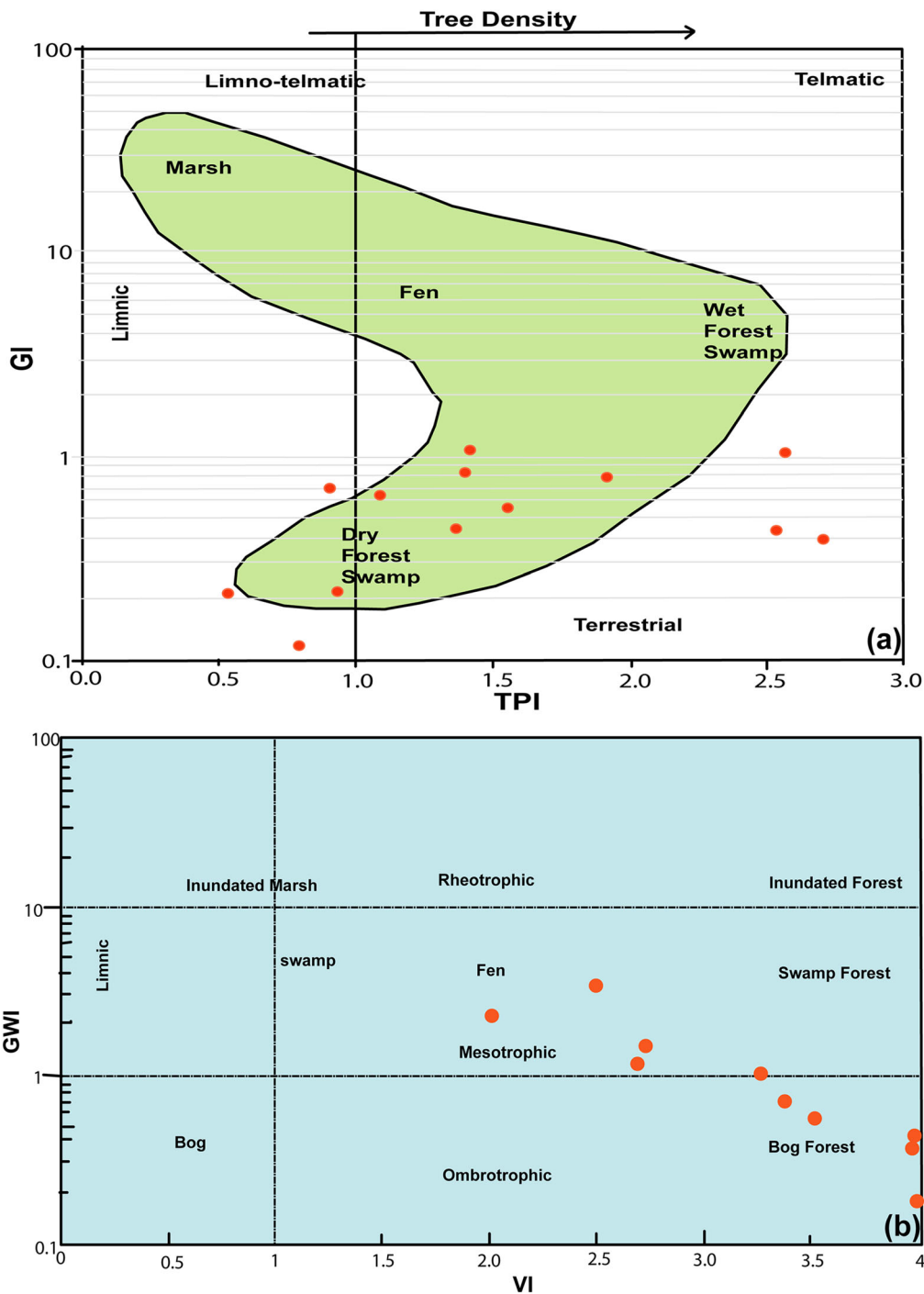
Figure 5. Coal facies diagram showing the paleodepositional and hydrological condition of the study area. **a** GI vs. TPI plot showing type of mire and depositional setting (after Diessel 1992). **b** VI vs. GWI plot showing hydrological and paleodepositional conditions (after Calder et al. 1991).

Table 3. Result of ultimate analysis of coals of Bikaner basin (Barsingsar lignite mines)

S. no.	Coalfield	Coal seam	Band no.	Dry basis					Dry ash-free basis					Atomic ratio	
				C%	H%	N%	S%	O%	C%	H%	N%	S%	O%	H/C	O/C
			Bottom												
1	Barsingsar	BS	1	62.81	4.66	0.91	0.97	21.61	69.04	5.13	1.00	1.07	23.76	0.89	0.26
2	Barsingsar	BS	2	62.87	4.49	1.03	0.55	19.98	70.71	5.05	1.15	0.62	22.47	0.86	0.24
3	Barsingsar	BS	3	63.52	4.05	1.09	0.48	17.67	73.17	4.66	1.25	0.56	20.36	0.76	0.21
4	Barsingsar	BS	4	51.90	3.72	0.99	0.34	20.39	67.11	4.81	1.28	0.44	26.36	0.86	0.29
5	Barsingsar	BS	5	59.92	4.05	1.03	0.34	20.31	69.96	4.73	1.21	0.39	23.72	0.81	0.25
6	Barsingsar	BS	6	52.37	4.42	0.83	0.30	21.00	66.36	5.60	1.05	0.38	26.61	1.01	0.30
7	Barsingsar	BS	7	22.52	2.90	0.45	0.18	17.56	51.65	6.65	1.03	0.41	40.27	1.55	0.58
8	Barsingsar	BS	8	37.19	3.56	0.73	0.24	22.19	58.20	5.58	1.14	0.37	34.71	1.15	0.45
9	Barsingsar	BS	9	61.88	3.87	1.09	0.26	19.83	71.19	4.45	1.25	0.30	22.81	0.75	0.24
10	Barsingsar	BS	10	43.32	3.74	0.80	0.28	17.80	65.69	5.68	1.21	0.43	26.99	1.04	0.31
11	Barsingsar	BS	11	46.83	3.24	1.27	0.65	22.06	63.24	4.37	1.71	0.88	29.79	0.83	0.35
			Top												
			Mean	51.38	3.88	0.93	0.42	20.04	66.03	5.16	1.21	0.53	27.08	0.96	0.32

C carbon, *H* hydrogen, *N* nitrogen, *S* sulfur, *O* oxygen

ingsar are provided in Tables 3 and 4, respectively, and the same are graphically illustrated in Figure 6. The results from ultimate analysis on dry basis (db) and dry ash-free (daf) along with the H/C and O/C atomic ratios are illustrated in Table 3. The concentrations of sulfur (0.18–0.97%, 0.42%), carbon (22.57–63.52%, 51.38%), nitrogen (0.45–1.27%, 0.93%), hydrogen (2.90–4.66%, 3.88%) and oxygen (17.56–22.19%, 20.04%) were obtained through ultimate analysis. The O/C (0.12–0.58, 0.32) and H/C (0.75–1.55, 0.96) ratios were calculated from the ultimate results. The results of proximate analysis on as-received basis, with the db and daf equivalents, are provided in Table 4. The lignites have low moisture content (7.03–13.65%; 9.86%), high volatile matter (32.58–44.22%, 36.70%), high fixed carbon (24.40–45.11%, 34.89) and high ash yield (4.38–33.58%, 18.56%).

Rock–Eval Pyrolysis

The type of organic matter, maturity and source rock potential can be inferred from geochemical data, such as Rock–Eval pyrolysis (Chen et al. 2016; Longbottom et al. 2016). The Rock–Eval data of Barsingsar lignites are shown in Table 5. The values of free hydrocarbon content (S_1), remaining hydrocarbon potential (S_2) and organic CO_2 (S_3) range from 0.74 to 2.63 mg HC/g, 51.62 to 142.12 mg HC/g and 6.53 to 18.91 mg HC/g, respectively, and total organic carbon (TOC) values range from 21.14 to

59.89 wt%. Hydrogen index (HI) and oxygen index (OI) values in Barsingsar range from 98 to 314 mg HC/g TOC and 27 to 43 mg CO_2/g TOC, respectively. The temperatures at maximum evolution of S_2 peak (T_{max}) are in the 422–432 °C range with mean of 424.73 °C.

Source Rock Potential and Thermal Maturity

The organic matter richness of a source rock enacts an important role in hydrocarbon generation, which can be inferred from TOC data (Peters et al. 2005; Sun et al. 2014). High TOC indicates oil generation from type III kerogen (Littke and Leythaeuser 1993). HI is another important geochemical parameter to characterize source rock. Low HI values (less than 200 mg HC/g TOC) reveal the presence of type III kerogen indicating gas generation from these lignites (Hunt 1996). On the contrary, high HI values (greater than 200 mg HC/g TOC) favor the generation of little oil (Hunt 1996). In the Barsingsar lignite, the values of HI are less than 200 mg HC/g TOC barring few samples (Table 5). From the HI data, it can be inferred that Barsingsar lignites generate mainly gases with limited quantity of liquid hydrocarbon. Significant values of TOC (av. 46 wt%) and HI (av. 188 mg HC/g TOC) in Barsingsar lignites make them favorable for the generation of hydrocarbon (mainly gases). The plot between S_2 and TOC indicates Barsingsar lignites to have a good hydrocarbon generative

Table 4. Result of proximate analysis (dry basis) of coals of Bikaner basin (Barsingsar lignite mines)

S. no.	Coalfield	Coal seam	Band no.	Proximate constituents (Ar)					Dry basis			DAF basis		
				Moisture	Ash	Volatile matter	Fixed carbon	Total	Ash	Volatile matter	Fixed carbon	Volatile matter	Fixed carbon	Total
			Bottom											
1	Barsingsar	BS	1	13.51	4.38	41.23	40.88	100.00	5.05	47.67	47.28	50.21	49.79	100
2	Barsingsar	BS	2	13.65	11.23	40.45	34.67	100.00	12.97	46.87	40.16	53.90	46.10	100
3	Barsingsar	BS	3	11.35	9.84	38.42	40.40	100.00	11.10	43.33	45.57	48.73	51.27	100
4	Barsingsar	BS	4	8.98	12.00	34.36	44.66	100.00	13.18	37.75	49.07	43.48	56.52	100
5	Barsingsar	BS	5	9.80	20.57	32.58	37.06	100.00	22.77	36.13	41.10	46.78	53.22	100
6	Barsingsar	BS	6	10.70	12.78	35.82	40.70	100.00	14.31	40.11	45.58	46.81	53.19	100
7	Barsingsar	BS	7	10.87	19.50	36.99	32.65	100.00	21.84	41.49	36.67	53.12	46.88	100
8	Barsingsar	BS	8	8.59	18.48	44.22	28.72	100.00	20.17	48.39	31.44	60.70	39.30	100
9	Barsingsar	BS	9	7.03	33.58	33.16	26.23	100.00	35.82	35.82	28.37	56.29	43.71	100
10	Barsingsar	BS	10	7.92	12.04	34.93	45.11	100.00	13.08	37.93	48.99	43.64	56.36	100
11	Barsingsar	BS	11	7.88	28.29	36.45	27.38	100.00	30.69	39.57	29.74	57.10	42.90	100
12	Barsingsar	BS	12	7.24	35.45	32.92	24.40	100.00	38.20	35.49	26.31	57.45	42.55	100
13	Barsingsar	BS	13	10.65	23.10	35.58	30.67	100.00	25.87	39.82	34.31	53.80	46.20	100
			Top											
			Mean	9.86	18.56	36.70	34.89	100.00	20.39	40.80	38.81	51.69	48.31	100

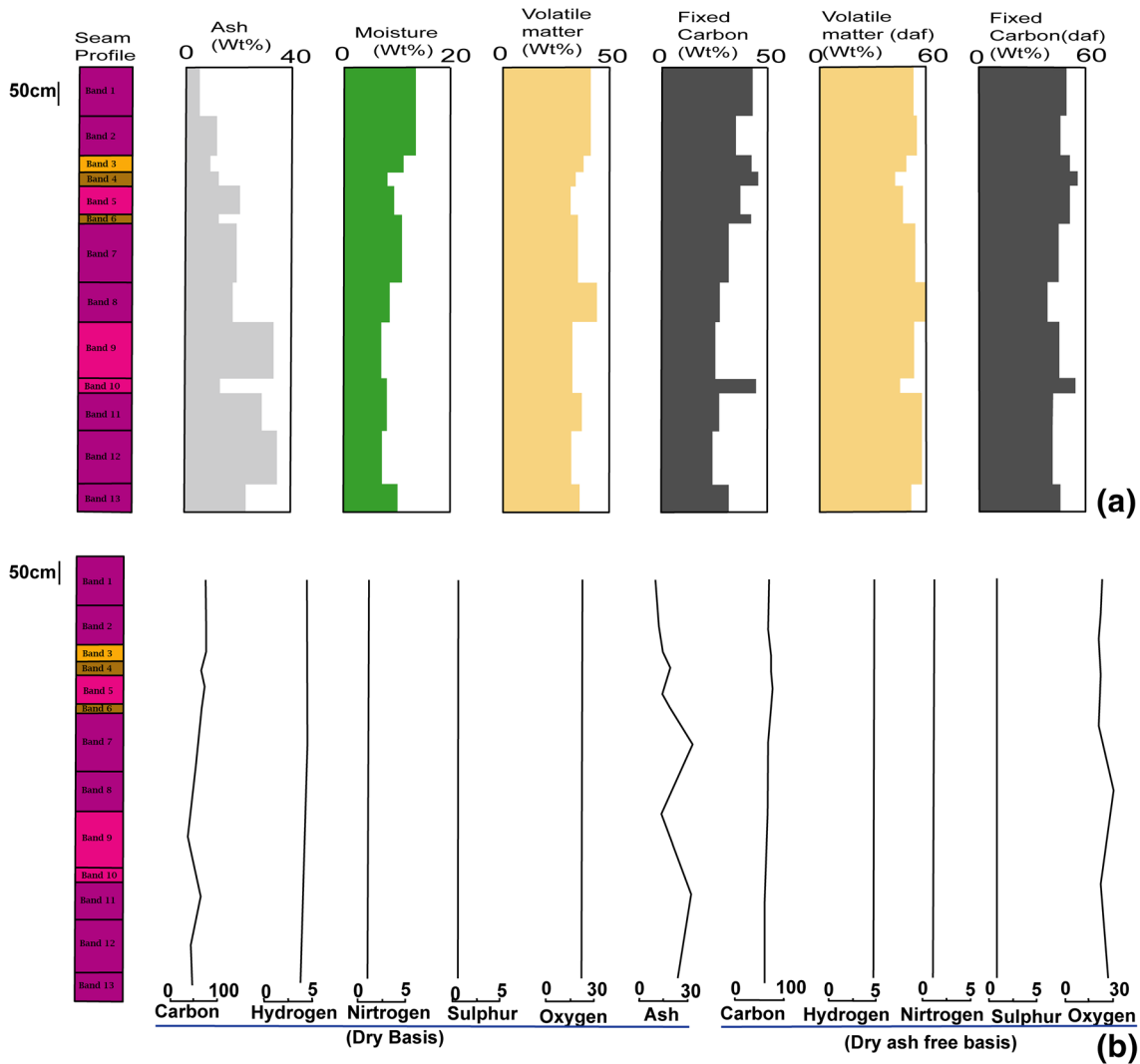*Ar* as-received basis, *Dr* dry basis, *DAF* dry ash-free basis

Figure 6. Graphical representation showing the variation of **a** proximate data and **b** ultimate data of Barsingsar lignites.

potential (Fig. 7a). All the studied samples show S_2/S_3 ratios more than 1, indicating that the Barsingsar lignites have the potential to generate hydrocarbons as per the guidelines of Peters and Cassa (1994). In addition, the high value of HI indicates the presence of liptinites and fluorescing huminite in the lignite samples (Singh et al. 2017b). Low OI values have been recorded due to stable oxygen moieties in the Barsingsar lignites (Varma et al. 2015a, b).

Furthermore, the plot of HI vs. T_{max} was used for the assessment of the maturity of organic matter and the type of kerogen present in the source rock (Mukhopadhyay et al. 1995). The plots of TOC vs. S_2 and T_{max} vs. HI fall within the mixed kerogen

type III/II, which indicates that the Barsingsar lignites are gas prone (Fig. 7b and c). The plot also suggests that the Barsingsar samples are thermally immature to marginally mature in nature (Fowler et al. 1991) (Fig. 7c). Additionally, to classify kerogen and to establish the evolution of organic matter, the H/C and O/C plots in van Krevelen's diagram were used (Erik 2011). The Barsingsar lignite samples fall mostly on the lignite to sub-bituminous coal range on the van Krevelen's diagram (after Singh et al. 2016b) and shows that the organic matter contains type III kerogen (Fig. 8).

Table 5. Result of Rock–Eval pyrolysis and oil yield calculation of lignites of the Bikaner basin (Barsingsar lignite mines)

S. no.	Coalfield	Coal seam	Band no.	T_{max} (C)	S_1 (mg HC/ g)	S_2 (mg HC/ g)	S_3 (mg HC/ g)	PI	S_2/S_3 (mg/g)	TOC (wt%)	HI (mg HC/g TOC)	OI (mg CO2/g TOC)	GP (mg/ g)
			Bottom										
1	Barsingsar	BS	1	424	1.02	91.48	18.91	0.01	4.84	53.55	171	35	92.5
2	Barsingsar	BS	2	422	2.33	120.09	16.27	0.02	7.38	59.33	202	27	122.42
3	Barsingsar	BS	3	423	0.88	64.19	16.85	0.01	3.81	59.89	107	28	65.07
4	Barsingsar	BS	4	423	1.01	61.54	14.72	0.02	4.18	48.62	127	30	62.55
5	Barsingsar	BS	5	425	1.22	96.38	15.64	0.01	6.16	50.85	190	31	97.6
6	Barsingsar	BS	6	426	2.15	142.12	15.37	0.01	9.25	49.71	286	32	144.27
7	Barsingsar	BS	7	426	1.61	66.47	6.53	0.02	10.18	21.14	314	31	68.08
8	Barsingsar	BS	8	422	1.43	65.33	12.27	0.02	5.32	34.24	191	36	66.76
9	Barsingsar	BS	9	422	0.74	51.62	15.59	0.01	3.31	52.41	98	30	52.36
10	Barsingsar	BS	10	427	2.63	96.24	10.97	0.03	8.77	37.8	255	29	98.87
11	Barsingsar	BS	11	432	0.85	54.37	17.4	0.02	3.12	40.52	134	43	55.22
			Top										
			Mean	424.73	1.44	82.71	14.59	0.02	6.03	46.19	188.64	32	
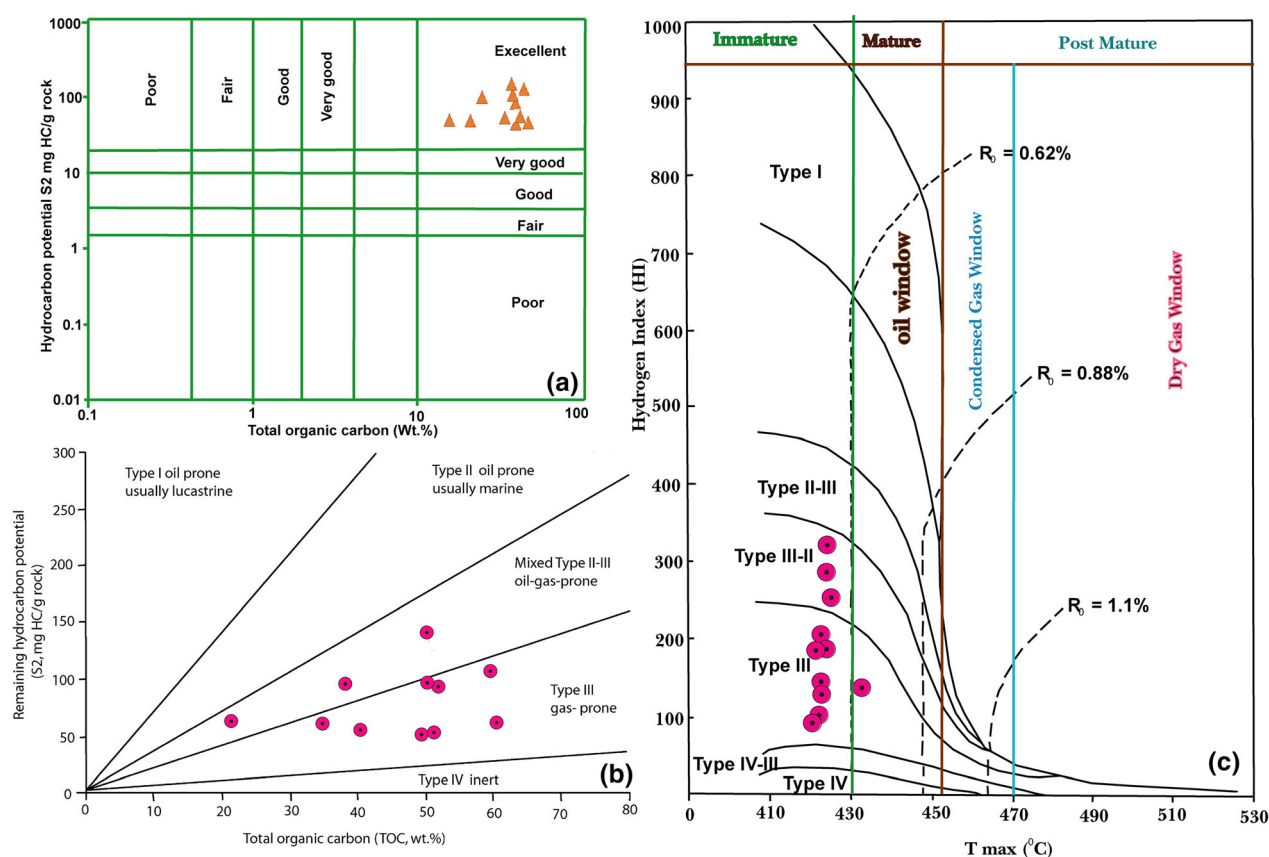
Figure 7. Plots for source rock potential, classification of kerogen type and maturity of organic matter based on pyrolysis result. **a** S_2 vs. TOC, **b** S_2 vs. TOC and HI vs. T_{max}, respectively, showing type III and mixed type II–III kerogens, thermally immature in nature and excellent hydrocarbon potential of the analyzed lignite samples in the Bikaner–Nagaur Basin.
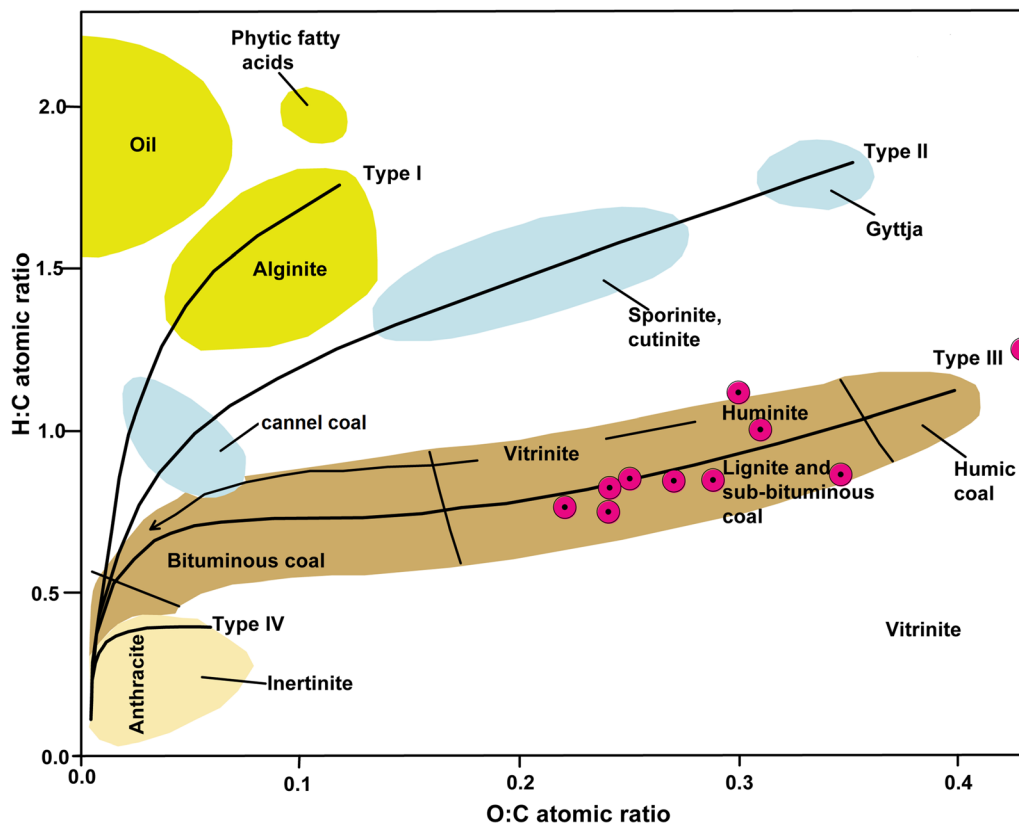
Figure 8. van Krevelen diagram showing plot between atomic ration H:C vs. O:C.

Mineralogy

Pyrite, carbonates and clay minerals were identified microscopically, while quartz, siderite, coesite, aragonite and rutile were identified by XRD. These minerals are expected to be the source of most of the major elements (Fig. 9). The concentrations of major oxides SiO_2 (41.07%), Al_2O_3 (34.23%), CaO (8.185%), MgO (3.02%), Na_2O (1.96%), FeO (1.30%), TiO_2 (0.75%), K_2O (0.15%), MnO (0.06%) and P_2O_5 (0.03%) are provided in Table 6. Concentrations (ppm) of selected trace elements (Rb, Sr, Zr, Cu, Zn, Pb, Ni, V and Cr) in the ash of lignite samples are given in Table 6.

The mineralogical study, including major oxides and trace elements of organic-rich sediments such as shale, coal/lignite and mudstone area, is a useful geochemical indicator to ascertain the paleodepositional and paleoclimatic condition of a Basin (Dai et al. 2005; Roy and Roser 2013; Xu et al. 2016). Important elements such as Si, Al and Ti were found associated with SiO_2, Al_2O_3 and TiO_2, respectively. The concentration of major oxides in lignites of

Barsingsar is predominated by SiO_2 (41.07%) and Al_2O_3 (34.23%), which suggest that the deposition of more clastic was by high energy deposition (Ayinla et al. 2017b). In addition, the cross-plot of SiO_2 vs. ($Al_2O_3 + K_2O + Na_2O$) was used to determine the paleodepositional conditions (Suttner and Dutta 1986). The cross-plot indicates deposition under semiarid to slightly arid climatic conditions (Fig. 10). The positive correlations for SiO_2–TiO_2, Al_2O_3–TiO_2 and K_2O–TiO_2 (Fig. 11) indicate that TiO_2 content is related to clay minerals.

The trace elements concentration of Sr, Rb and V was used for discrimination between seawater and freshwater (Makeen et al. 2015). On the other hand, V, Ni, Cu and Cr are redox-sensitive elements and were used to decipher the paleodepositional condition during sedimentation (Mohialdeen and Raza 2013; Armstrong-Altrin and Machain-Castillo 2016). The trace element distribution is dominated by Rb, Sr and Zr with moderate concentration of Cu, Zn, Pb, Ni, V and Cr. Vanadium (V) and nickel (Ni) are important trace elements usually incorporated with organic matter during early diagenetic stage and are
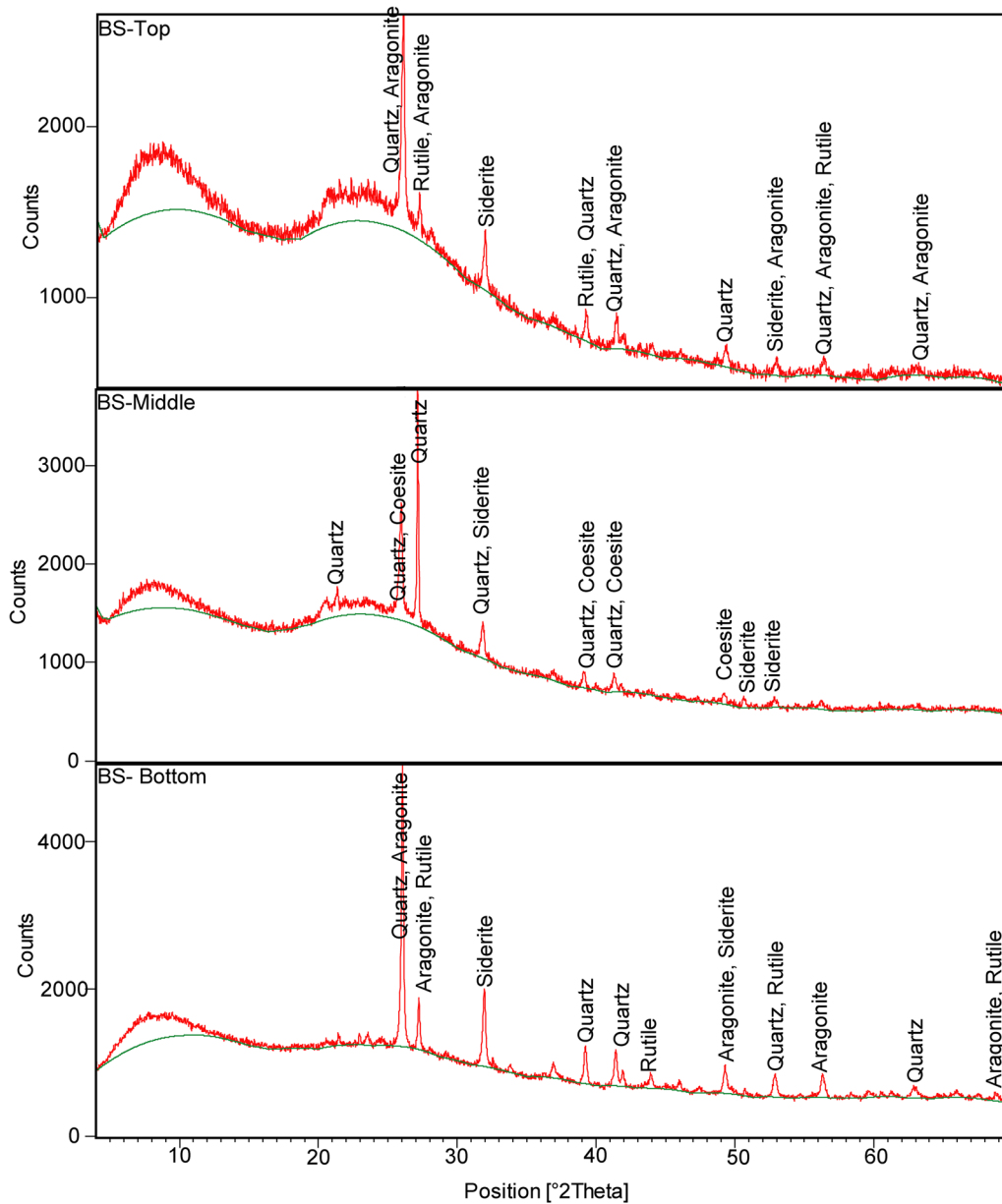
Figure 9. X-ray diffractogram (XRD) of ash of three composite lignite samples according to their lithotype of Barsingsar lignite.

useful indicators of redox conditions during the sedimentation process (Rimmer 2004; Galarraga et al. 2008). The bivariant plot of V vs. Ni (Fig. 12a) shows that the deposition of organic matter took place in a deltaic setting under sub-oxic to oxic condition. Similarly, the low sulfur content coupled with moderate V/(V + Ni) ratio (Fig. 12b) further supports sub-oxic condition during the sedimentation of the organic matter.

In addition, to detect various minerals as well as to delineate carbohydrogenated structure (aromatic and aliphatic) and heteroatomic functions (mainly oxygenated), FT-IR technique was used (Georgakopoulos et al. 2003). The details of observed organic and inorganic function groups with corresponding wave numbers are given in Table 7 and illustrated in Figure 13. The sharp peaks at 3696, 3695, 3694, 3693, 3654, 3653, 3652, 3649, 3621, 3620,

Table 6. Mineralogical analysis and trace element concentration of lignite ash using XRF technique

Sample/band	Concentrations of oxide of major elements in weight %										Trace elements concentrations in ppm								
Oxide/elements	SiO_2	Al_2O_3	CaO	MgO	Na_2O	FeO	TiO_2	K_2O	MnO	P_2O_5	Rb	Sr	Zr	Cu	Zn	Pb	Ni	V	Cr
Band 1	38.70	31.79	9.44	4.12	2.58	1.60	0.69	0.17	0.07	0.04	1367.959	1164.613	288.118	162.273	250.905	127.834	119.222	62.479	76.775
Band 2	41.32	33.75	7.95	3.47	2.32	1.14	0.73	0.16	0.06	0.03	1199.113	1029.921	270.567	171.771	138.396	134.075	78.771	69.072	75.989
Band 3	45.59	38.83	2.39	1.16	1.18	1.13	0.93	0.16	0.02	0.03	479.614	442.649	209.511	84.427	73.561	95.61	53.291	91.19	64.355
Band 4	38.66	32.55	12.95	3.34	1.76	1.35	0.66	0.12	0.08	0.03	2050.86	1725.242	343.348	123.394	65.62	100.976	38.716	59.297	59.924
Mean	41.07	34.23	8.18	3.02	1.96	1.30	0.75	0.15	0.06	0.03	1274.39	1090.61	277.89	135.47	132.12	114.62	72.50	70.51	69.26
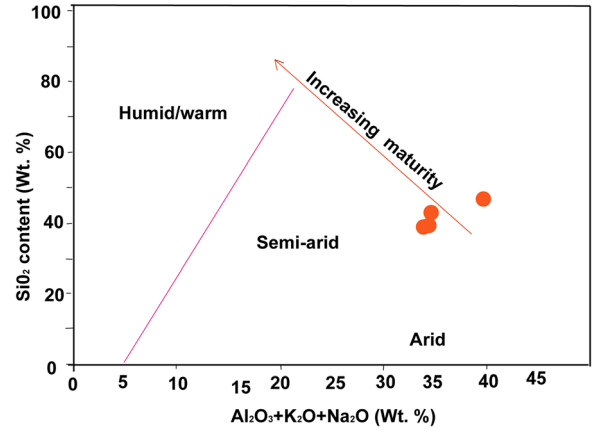
Figure 10. Plot of SiO_2 vs. $(Al_2O_3 + K_2O + Na_2O)$ showing the paleoclimatic condition during sedimentation of the studied lignite samples (adapted after Suttner and Dutta 1986).
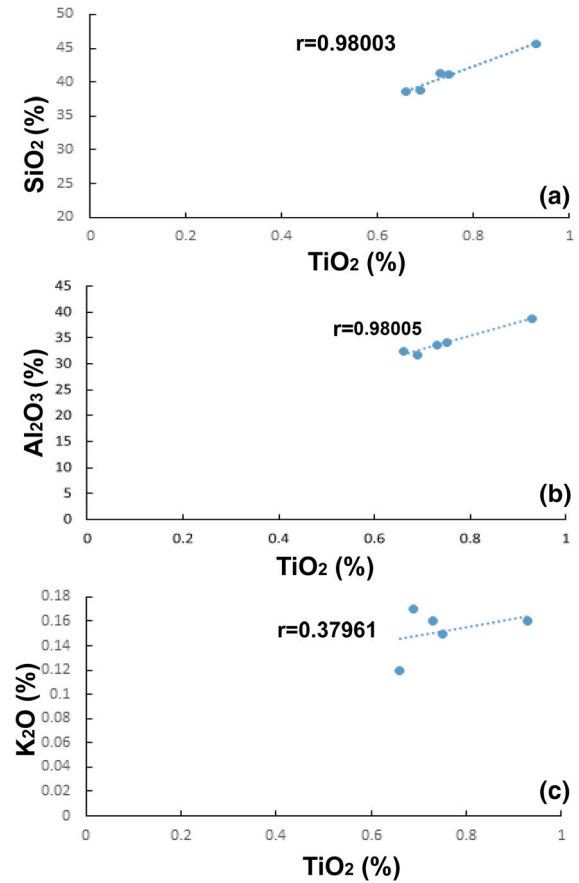
Figure 11. Correlation between major element oxides for Barsingsar lignites. **a** SiO_2 vs. TiO_2, **b** Al_2O_3 vs. TiO_2, **c** K_2O vs. TiO_2.

3619 and 3618 cm^{-1} are observed due to O–H stretching vibrations of hydrogen-bonded hydroxyl groups (Oikonomopoulos et al. 2010; Chen et al. 2015; Equeenuddin et al. 2016). In addition, sharp peaks of medium intensity at 3000–2800, 2850 and 2920 cm^{-1} represent the C-H aliphatic stretching region (Ganz and Kalkreuth 1991; Oikonomopoulos et al. 2010; Chen et al. 2015). Aliphatic and alicyclic CH$_3$, CH$_2$ and CH groups were observed at 2853 cm^{-1}. The sharp peaks of 1031 and 1300–1000 cm^{-1} represent lignin and cellulose region (C-O-H deformation in cellulose) (Oikonomopoulos et al. 2010). The wave number 1008 cm^{-1} is attributed to Si–O–Si stretching (Equeenuddin et al. 2016). On the other hand, bands at 3652, 3620, 1095, 1034, 1031, 1009, 914, 910, 690 and 689 cm^{-1} represent the dominance of kaolinite mineral with the presence of bands 750 and 790 cm^{-1} representing marcasite and quartz, respectively (Chen et al. 2015).
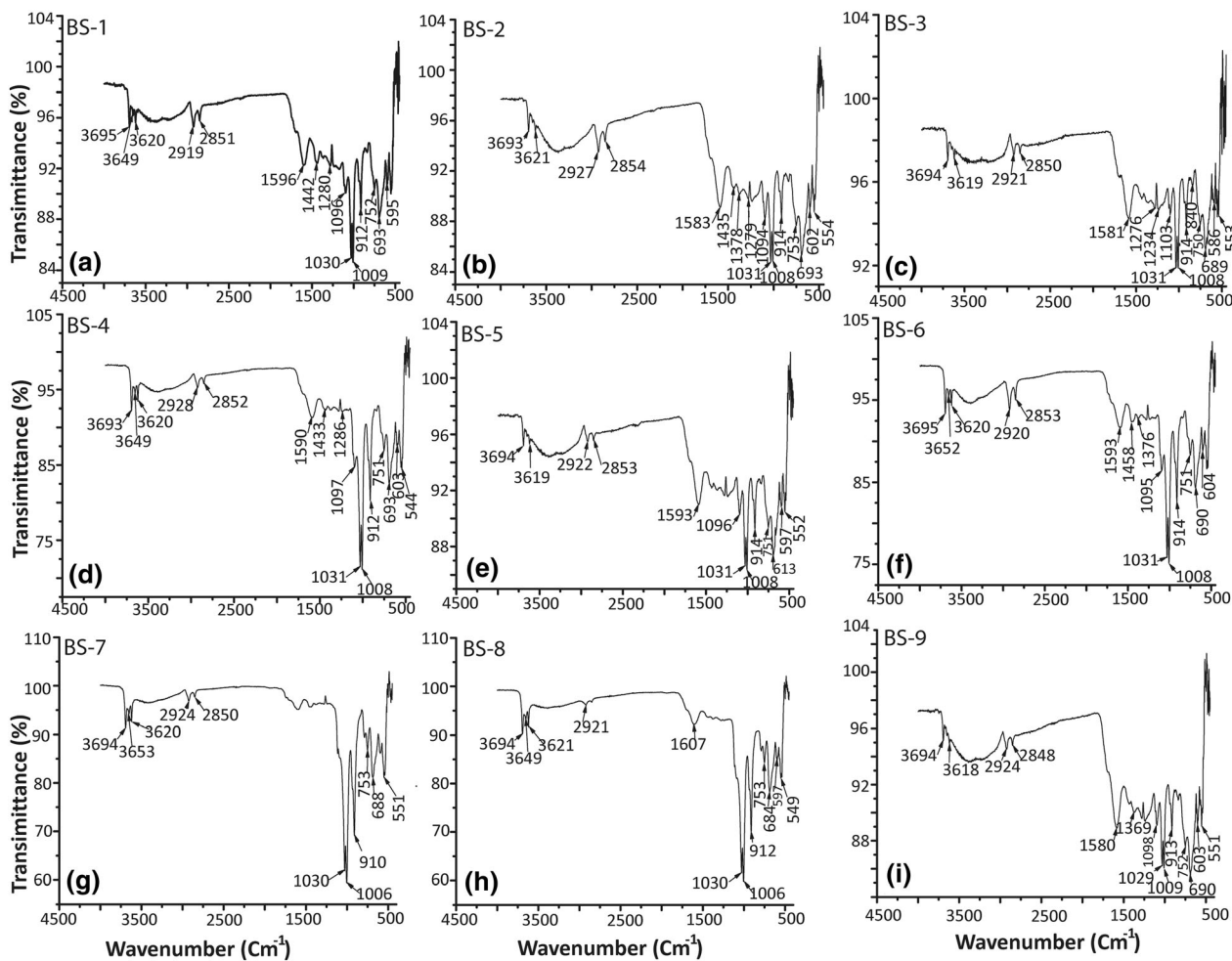
Figure 12. a Plot of vanadium vs. nickel in ppm showing the depositional condition for the analyzed samples (adapted after Galarraga et al. 2008). **(b)** Plot between trace element ratios of V/(V + Ni) vs. total sulfur content (wt%) of the analyzed samples (Galarraga et al. 2008).

Table 7. Band assignments for the infrared spectra of Barsingsar lignite (Wang and Griffiths 1985; Ganz and Kalkreuth 1991; Oikonomopoulos et al. 2010; Chen et al. 2015; Varma et al. 2015a, b; Equeenuddin et al. 2016; Choudhury et al. 2017)

Organic functional groups		Inorganic functional groups	
Wavenumber (cm^{-1})	Assignment	Wavenumber (cm^{-1})	Assignment
3100–3700, 3621	O–H stretching vibrations of hydrogen-bonded hydroxyl groups	3600–3800	Clay minerals
3400–3800	Aromatic O–H (phenolic)	3652, 3620, 1095, 1034, 1031, 1009, 914, 910, 690, 689	Kaolinite
3000–3100	Aromatic C–H stretching	3620	Illite
3000–2800, 2850, 2920, 2924	C–H aliphatic stretching region	1006	Glauconite
2853	Aliphatic and alicyclic CH$_3$, CH$_2$ and CH groups	790	Quartz
1560–1590	Carboxyl and carbonyl groups	750	Marcasite
1300–1000, 1031	Cellulose and lignin region (C–O–H deformation in cellulose)		
1300–1100	C–O stretch and O–H bend in phenoxy structures, ethers		
1100–1000	Aliphatic ethers, alcohols		
1008	Si–O–Si stretching		
700–900	Aromatic C–H out-of-plane region		
912, 751	Aromatic structures		
690	Stretching of S–S bonds of sulfides and C–S bonds thiols		

Figure 13. FTIR spectra of studied lignite samples of Barsingsar.

CONCLUSIONS

The following conclusions were drawn from the petrographic and geochemical study of Paleogene lignites in the Palana Formation.

- These lignites have relatively high huminite and inertinite content with respect to liptinite, along with significant amounts of mineral matter. High concentration of detrohuminite indicates abundance of herbaceous plants, while substantial textinite concentration indicates high degree of cell tissue preserved under relatively dry forest condition.
- The bands of high inertinite concentration indicate periodic dry (oxic) conditions during peat accumulation. GWI and VI indicate that these lignites were formed from a bog forest under ombrotrophic to mesotrophic mire condition.
- Low sulfur content (0.18–0.97%, < 1% S) recorded in the Barsingsar indicates influence of fluvial environment in the region.
- The low huminite reflectance (%R_{om}) and T_{max} values of Barsingsar lignite indicate their immaturity, which is also reflected in the geochemical data. Lignite contains a mixed kerogen type III/II, which indicates potential for lighter hydrocarbon.
- The ash of these lignites contains mainly quartz, siderite, coesite, aragonite and rutile. SiO_2 (41.07%) and Al_2O_3 (34.23%) are the predominant oxides, which suggest deposi-

tion of more clastic by high energy deposition. The concentrations of trace elements indicate organic matter deposited under suboxic to oxic condition in a deltaic setting. The FT-IR analysis of raw lignite samples shows the dominance of kaolinite minerals along with quartz and marcasite.

ACKNOWLEDGMENTS

REFERENCES

Abdullah, W. H. (2003). Coaly source rocks of NW Borneo: Role of suberinite and bituminite in generation and expulsion. *Bulletin of Geological Society of Malaysia, 47,* 119–129.

Ahmad, A., Hakimi, M. H., & Chaudhry, M. N. (2015). Geochemical and organic petrographic characteristics of low-rank coals from Thar coalfield in the Sindh Province, Pakistan. *Arabian Journal of Geosciences, 8*(7), 5023–5038.

Armstrong-Altrin, J. S., & Machain-Castillo, M. L. (2016). Mineralogy, geochemistry, and radiocarbon ages of deep-sea sediments from the Gulf of Mexico, Mexico. *Journal of South American Earth Sciences, 71,* 182–200.

ASTM D5373-08. (1993). Standard test methods for instrumental determination of carbon, hydrogen, and nitrogen in laboratory samples of coal, pp. 1–11.

ASTM D7708-11. (2011). Standard test method for microscopical determination of the reflectance of vitrinite dispersed in sedimentary rocks.

Ayinla, H. A., Abdullah, W. H., Makeen, Y. M., Abubakar, M. B., Jauro, A., Yandoka, B. M. S., et al. (2017a). Petrographic and geochemical characterization of the Upper Cretaceous coal and mudstones of Gombe Formation, Gongola sub-basin, northern Benue trough Nigeria: Implication for organic matter preservation, paleodepositional environment and

tectonic settings. *International Journal of Coal Geology, 180,* 67–82.

Ayinla, H. A., Abdullah, W. H., Makeen, Y. M., Abubakar, M. B., Jauro, A., Yandoka, B. M. S., et al. (2017b). Source rock characteristics, depositional setting and hydrocarbon generation potential of Cretaceous coals and organic rich mudstones from Gombe Formation, Gongola Sub-basin, Northern Benue Trough, NE Nigeria. *International Journal of Coal Geology, 173,* 212–226.

Baboolal, A. A., Littke, R., Wilson, B., Stock, A. T., & Knight, J. (2016). Petrographical and geochemical characterization of lignites, sub-bituminous coals and carbonaceous sediments from the Erin Formation, Southern Basin, Trinidad—Implications on microfacies, depositional environment and organic matter alteration. *International Journal of Coal Geology, 163,* 112–122.

Bechtel, A., Karayiğit, A. I., Bulut, Y., Mastalerz, M., & Sachsenhofer, R. F. (2016). Coal characteristics and biomarker investigations of Dombayova coals of Late Miocene–Pliocene age (Afyonkarahisar-Turkey). *Organic Geochemistry, 94,* 52–67.

Bechtel, A., Reischenbacher, D., Sachsenhofer, R. F., Gratzer, R., Lücke, A., & Püttmann, W. (2007a). Relations of petrographical and geochemical parameters in the middle Miocene Lavanttal lignite (Austria). *International Journal of Coal Geology, 70,* 325–349.

Bechtel, A., Sachsenhofer, R. F., Markic, M., Gratzer, R., Lucke, A., & Puttmann, W. (2003). Paleoenvironmental implications from biomarker and stable isotope investigations on the Pliocene Velenje lignite seam (Slovenia). *Organic Geochemistry, 34,* 1277–1298.

Bechtel, A., Widera, M., Sachsenhofer, R. F., Gratzer, R., Lücke, A., & Woszczyk, M. (2007b). Biomarker and stable carbon isotope systematics of fossil wood from the second Lusatian lignite seam of the Lubstów deposit (Poland). *Organic Geochemistry, 38,* 1850–1864.

Bhandari, A. (1999). Phanerozoic stratigraphy of western Rajasthan India: A review. In P. Kataria (Ed.), *Geology of Rajasthan: Status and perspective* (pp. 126–174). Udaipur: MLS University.

Bhattacharya, S., & Dutta, S. (2015). Neoproterozoic-Early Cambrian biota and ancient niche: A synthesis from molecular markers and palynomorphs from Bikaner–Nagaur-Nagaur Basin, western India. *Precambrian Research, 266,* 361–374.

BIS. (2003). Methods of test for coal and coke (2nd revision of IS: 1350). Part I, Proximate analysis. Bureau of Indian Standard (pp. 1–29).

Calder, J. H., Gibling, M. R., & Mukhopadhyay, P. K. (1991). Peat formation in a Westphalian B piedmont setting, Cumberland basin, Nova Scotia: Implications for the maceral-based interpretation of rheotrophic and raised paleomires. Contribution series No. 91-002.

Chen, Y., Zou, C., Mastalerz, M., Hu, S., Gasaway, C., & Tao, X. (2015). Applications of micro-Fourier transform infrared spectroscopy (FTIR) in the geological sciences—A review. *International Journal of Molecular Sciences, 16*(12), 30223–30250.

Chen, Z., Jiang, C., Lavoie, D., & Reyes, J. (2016). Model-assisted Rock-Eval data interpretation for source rock evaluation: Examples from producing and potential shale gas resource plays. *International Journal of Coal Geology, 165,* 290–302.

Chou, C. L. (2012). Sulfur in coals: A review of geochemistry and origins. *International Journal of Coal Geology, 100,* 1–13.

Choudhury, R., Saikia, J., & Saikia, B. K. (2017). Mineralogical and ash geochemical studies of coal-mine shale and its hydrocarbon potential: A case study of shale from Makum coalfield, Northeast India. *Journal of Geological Society of India, 90*(3), 329–334.

Dai, S., Ren, D., Tang, Y., Yue, M., & Hao, L. (2005). Concentration and distribution of elements in Late Permian coals from western Guizhou Province, China. *International Journal of Coal Geology, 61,* 119–137.

Diessel, C. F. K. (1986). On the correlation between coal facies and depositional environments. In *Proceeding 20th symposium of department geology, University of New Castle, New South Wales* (pp. 19–22).

Diessel, C. F. K. (1992). *Coal-bearing depositional systems*. Berlin: Springer.

Đoković, N., Mitrović, D., Životić, D., Bechtel, A., Sachsenhofer, R. F., Matić, V., et al. (2018). Petrographical and organic geochemical study of the lignite from the Smederevsko Pomoravlje field (Kostolac Basin, Serbia). *International Journal of Coal Geology, 195,* 139–171.

Dutta, S., Mathews, R. P., Singh, B. D., Tripathi, S. K. M., Singh, A., Saraswati, P. K., et al. (2011). Petrology, palynology and organic geochemistry of Eocene lignite of Matanomadh, Kutch Basin, western India: Implications to depositional environment and hydrocarbon source potential. *International Journal of Coal Geology, 85,* 91–102.

Equeenuddin, S. M., Tripathy, S., Sahoo, P. K., & Ranjan, A. (2016). Geochemical characteristics and mode of occurrence of trace elements in coal at West Bokaro coalfield. *International Journal of Coal Science & Technology, 3*(4), 399–406.

Erik, N. Y. (2011). Hydrocarbon generation potential and Miocene–Pliocene palaeoenvironment of the Kangal Basin (Central Anatolia, Turkey). *Journal of Asian Earth Sciences, 42,* 1146–1162.

Farrimond, P., Naidu, B. S., Burley, S. D., Dolson, J., Whiteley, N., & Kothari, V. (2015). Geochemical characterization of oils and their source rocks in the Barmer Basin, Rajasthan, India. *Petroleum Geoscience, 21*(4), 301–321.

Fowler, M. G., Gentzis, T., Goodarzi, F., & Foscolos, A. E. (1991). The petroleum potential of some Tertiary lignites from northern Greece as determined using pyrolysis and organic petrological techniques. *Organic Geochemistry, 17,* 805–826.

Galarraga, F., Reategui, K., Martïnez, A., Martínez, M., Llamas, J. F., & Márquez, G. (2008). V/Ni ratio as a parameter in palaeoenvironmental characterization of non-mature medium-crude oils from several Latin American basins. *Journal of Petroleum Science and Engineering, 61,* 9–14.

Ganz, H. H., & Kalkreuth, W. (1991). IR classification of kerogen type, thermal maturation, hydrocarbon potential and lithological characteristics. *Journal of Southeast Asian Earth Sciences, 5*(1–4), 19–28.

Georgakopoulos, A., Iordanidis, A., & Kapina, V. (2003). Study of low rank Greek coals using FTIR spectroscopy. *Energy Sources, 25,* 995–1005.

Guo, Q., Littke, R., & Zieger, L. (2018). Petrographical and geochemical characterization of sub-bituminous coals from mines in the Cesar-Ranchería Basin, Colombia. *International Journal of Coal Geology, 191,* 66–79.

Hakimi, M. H., Abdullah, W. H., Sia, S. G., & Makeen, Y. M. (2013). Organic geochemical and petrographic characteristics of Tertiary coals in the northwest Sarawak, Malaysia: Implications for palaeoenvironmental conditions and hydrocarbon generation potential. *Marine and Petroleum Geology, 48,* 31–46.

Hasiah, A. W. (1999). Oil-generating potential of Tertiary coals and other organic-rich sediments of the Nyalau Formation, onshore Sarawak. *Journal of Asian Earth Sciences, 17,* 255–267.

Hunt, J. H. (1996). *Petroleum geology and geochemistry* (2nd ed., p. 743). New York: Freeman.

International Committee for Coal and Organic Petrology. (1993). *International handbook of coal petrography, 3rd Supplement to 2nd edition*. Newcastle upon Tyne: University of Newcastle upon Tyne.

International Committee for Coal and Organic Petrology. (2001). The new inertinite classification (ICCP System 1994). *Fuel, 80,* 459–471.

International Committee for Coal and Organic Petrology. (2005). Classification of huminite (ICCP System 1994). *International Journal of Coal Geology, 62,* 85–106.

International Committee for Coal and Organic Petrology. (2017). Classification of liptinite (ICCP System 1994). *International Journal of Coal Geology, 169,* 40–61.

ISO 7404-5. (2009). *Methods for the petrographic analysis of bituminous coal and anthracite—Part 5: Methods of determining microscopically the reflectance of vitrinite* (p. 11). Geneva: International Organization for Standardization ISO.

Johnston, M. N., Eble, C. F., O'Keefe, J. M., Freeman, R. L., & Hower, J. C. (2017). Petrology and palynology of the Middle Pennsylvanian Leatherwood coal bed, Eastern Kentucky: Indications for depositional environments. *International Journal of Coal Geology, 181,* 23–38.

Kalkreuth, W., Kotis, T., Papanicolaou, C., & Kokkinakis, P. (1991). The geology and coal petrology of a Miocene lignite profile at Meliadi Mine Katerini, Greece. *International Journal of Coal Geology, 17,* 51–67.

Karayiğit, Aİ., Littke, R., Querol, X., Jones, T., Oskay, R. G., & Christanis, K. (2017). The Miocene coal seams in the Soma Basin (W. Turkey): Insights from coal petrography, mineralogy and geochemistry. *International Journal of Coal Geology, 173,* 110–128.

Koukouzas, N., Kalaitzidis, S. P., & Ward, C. R. (2010). Organic petrographical, mineralogical and geochemical features of the Achlada and Mavropigi lignite deposits, NW Macedonia, Greece. *International Journal of Coal Geology, 83,* 387–395.

Kumar, M., Spicer, R. A., Spicer, T. E., Shukla, A., Mehrotra, R. C., & Monga, P. (2016). Palynostratigraphy and palynofacies of the early Eocene Gurha lignite mine, Rajasthan, India. *Palaeogeography, Palaeoclimatology, Palaeoecology, 461,* 98–108.

Littke, R., & Leythaeuser, D. (1993). Migration of oil and gas in coals. In B. E. Law & D. D. Rice (Eds.), *Hydrocarbons from coal* (Vol. 38, pp. 219–236). Tulsa: American Association of Petroleum Geologist.

Longbottom, T. L., Hockaday, W. C., Boling, K. S., Li, G., Letourmy, Y., Dong, G., et al. (2016). Organic structural properties of kerogen as predictors of source rock type and hydrocarbon potential. *Fuel, 184,* 792–798.

Makeen, Y. M., Abdullah, W. H., & Hakimi, M. H. (2015). The origin, type and preservation of organic matter of the Barremiane Aptian organic-rich shales in the Muglad Basin, Southern Sudan, and their relation to paleoenvironmental and paleoclimate conditions. *Marine and Petroleum Geology, 65,* 187–197.

Mohialdeen, M. J., & Raza, S. M. (2013). Inorganic geochemical evidence for the depositional facies associations of the Upper Jurassic Chia Gara Formation in NE Iraq. *Arabian Journal of Geoscience, 6,* 4755–4770.

Mukherjee, A. K., Alum, M. M., Mazumdar, S. K., Haque, R., & Gowrisankaran, S. (1992). Physico-chemical properties and petrographic characteristics of the Kapurdi lignite deposit, Barmer Basin, Rajasthan, India. *International Journal of Coal Geology, 21,* 31–44.

Mukhopadhyay, P. (1989). Organic petrography and organic geochemistry of Tertiary Coals from Texas in relation to depositional environment and hydrocarbon generation. Report of Investigations, Bureau of Economic Geology, Texas (pp. 118).

Mukhopadhyay, P. K. (1986). Petrography of selected Wilcox and Jockson Group lignites from Tertiary of Texas. In: R. B. Finkelman & D. J. Casagrade (Eds.), *Geology of gulf coast lignites, 1986, Annual meeting, Geological Society of America, Coal Geology Division, Field Trip* (pp. 126–145).

Mukhopadhyay, P. K., Wade, J. A., & Kruge, M. A. (1995). Organic facies and maturation of Jurassic/Cretaceous rocks, and possible oil-source rock correlation based on pyrolysis of asphaltenes, Scotion Basin, Canada. *Organic Geochemistry, 22,* 85–104.

O'Keefe, J. M. K., Bechtel, A., Christanis, K., Dai, S., Di Michele, W. A., Eble, C. F., et al. (2013). On the fundamental difference between coal rank and coal type. *International Journal of Coal Geology, 118,* 58–87.

Oikonomopoulos, I., Perraki, Th, & Tougiannidis, N. (2010). FTIR study of two different lignite lithotypes from neocene Achlada lignite deposits in NW Greece. *Bulletin of the Geological Society of Greece, 43,* 2284–2293.

Oskay, R. G., Christanis, K., Inaner, H., Salman, M., & Taka, M. (2016). Palaeoenvironmental reconstruction of the eastern part of the Karapınar-Ayrancı coal deposit (Central Turkey). *International Journal of Coal Geology, 163,* 100–111.

Pareek, H. S. (1981). Basin configuration and sedimentary stratigraphy of western Rajasthan. *Journal of Geological Society of India, 22,* 517–527.

Pareek, H. S. (1984). *Pre-quaternary geology and mineral resources of northwestern Rajasthan* (Vol. 115). Calcutta: Memoir Geological Survey of India.

Paul, S., & Dutta, S. (2016). Terpenoid composition of fossil resins from western India: New insights into the occurrence of resin-producing trees in Early Paleogene equatorial rainforest of Asia. *International Journal of Coal Geology, 167,* 65–74.

Peters, K. E., & Cassa, M. R. (1994). Applied source rock geochemistry. In L. B. Magoon & W. G. Dow (Eds.), *The petroleum system—From source to trap* (Vol. 60, pp. 93–120). Tulsa: Memoir American Association of Petroleum Geologists.

Peters, K. E., Walters, C. C., & Moldowan, J. M. (2005). *The biomarker guide: Biomarkers and isotopes in petroleum exploration and earth history* (2nd ed.). Cambridge: Cambridge University Press.

Prasad, V., Farooqui, A., Tripathi, S. K. M., Garg, R., & Thakur, B. (2009). Evidence of late Palaeocene-early Eocene equatorial rain forest refugia in southern Western Ghats, India. *Journal of Biosciences, 34,* 777–797.

Radhwani, M., Bechtel, A., Singh, V. P., Singh, B. D., & Mannaï-Tayech, B. (2018). Petrographic, palynofacies and geochemical characteristics of organic matter in the Saouef Formation (NE Tunisia): Origin, paleoenvironment, and economic significance. *International Journal of Coal Geology, 187,* 114–130.

Raju, S. V., & Mathur, N. (2013). Rajasthan lignite as a source of unconventional oil. *Current Science, 104*(6), 752–757.

Rimmer, S. M. (2004). Geochemical paleoredox indicators in Devonian–Mississippian black shales, central Appalachian Basin (USA). *Chemical Geology, 206,* 373–391.

Roy, A. B., & Jakhar, S. R. (2002). *Geology of Rajasthan (northwest India), precambrian to Recent* (p. 421). Jodhpur: Scientific Publishers (India).

Roy, D. K., & Roser, B. P. (2013). Climatic control on the composition of Carboniferous–Permian Gondwana sediments, Khalaspir basin, Bangladesh. *Gondwana Research, 23,* 1163–1171.

Shivanna, M., Singh, A., Singh, B. D., Singh, V. P., Matthews, R. P., & Souza, A. (2016). Peat biomass degradation: Evidence from fungal and faunal activity in carbonized wood from the Eocene sediments of western India. *Palaeoworld, 26*(3), 531–542.

Shivanna, M., & Singh, H. (2016). Depositional environment and hydrocarbon potential of marginal marine sediments of Eocene from western India: A palynofacies perspective. *Marine and Petroleum Geology, 73,* 311–321.

Shukla, A., Mehrotra, R. C., Spicer, R. A., Spicer, T. E., & Kumar, M. (2014). Cool equatorial terrestrial temperatures and the South Asian monsoon in the Early Eocene: Evidence from the Gurha Mine, Rajasthan, India. *Palaeogeography, Palaeoclimatology, Palaeoecology, 412,* 187–198.

Singh, P. K. (2012). Petrological and geochemical considerations to predict oil potential of Rajpardi and Vastan Lignite deposits of Gujarat, Western India. *Journal of the Geological Society of India, 80*(6), 759–770.

Singh, A. V., Bhargava, P. K., Singh, R., & Menaria, K. L. (2012). The selective oil agglomeration of combustibles in fines of low grade lignite of Barmer Rajasthan (India). *Energy Sources, Part A: Recovery, Utilization, and Environmental Effects, 34*(16), 1491–1496.

Singh, A. K., & Kumar, A. (2017a). Liquefaction behavior of Eocene lignites of Nagaur Basin, Rajasthan, India: A petrochemical approach. *Energy Sources, Part A: Recovery, Utilization, and Environmental Effects, 39*(15), 1686–1693.

Singh, A. K., & Kumar, A. (2017b). Petro-chemical characterisation and depositional paleoenvironment of lignite deposits of Nagaur, Western Rajasthan, India. *Environmental Earth Science, 76*(20), 692.

Singh, A. K., & Kumar, A. (2018a). Petrographic and Geochemical study of Gurha lignites, Bikaner Basin, Rajasthan, India: Implications for thermal maturity, hydrocarbon generation potential and paleodepositional environment. *Journal of Geological Society of India, 92*(1), 27–35.

Singh, A. K., & Kumar, A. (2018b). Organic geochemical characteristics of Nagaur lignites, Rajasthan, India and their implication on thermal maturity and paleoenvironment. *Energy Sources, Part A: Recovery, Utilization, and Environmental Effects, 40*(15), 1842–1851.

Singh, A. K., Kumar, A., & Hakimi, M. H. (2018). Organic geochemical and petrographical characteristics of the Nagaur lignites, Western Rajasthan, India and their relevance to liquid hydrocarbon generation. *Arabian Journal of Geosciences, 11,* 406.

Singh, P. K., Rajak, P. K., Singh, M. P., Naik, A. S., Singh, V. K., Raju, S. V., et al. (2015). Environmental Geochemistry of selected elements in lignite from Barsingsar and Gurha Mines of Rajasthan, Western India. *Journal of Geological Society of India, 86*(1), 23–32.

Singh, P. K., Rajak, P. K., Singh, V. K., Singh, M. P., Naik, A. S., & Raju, S. V. (2016a). Studies on thermal maturity and hydrocarbon potential of lignites of Bikaner–Nagaur–Nagaur basin, Rajasthan. *Energy Exploration & Exploitation, 34*(1), 140–157.

Singh, A., Shivanna, M., Mathews, R. P., Singh, B. D., Singh, H., Singh, V. P., et al. (2017a). Paleoenvironment of Eocene lignite bearing succession from Bikaner–Nagaur-Nagaur Basin, western India: Organic petrography, palynology, palynofacies and geochemistry. *International Journal of Coal Geology, 181,* 87–102.

Singh, V. P., Singh, B. D., Mathews, R. P., Singh, A., Mendhe, V. A., Singh, P. K., et al. (2017b). Investigation on the lignite deposits of Surkha mine (Saurashtra Basin, Gujarat), western India: Their depositional history and hydrocarbon generation potential. *International Journal of Coal Geology, 183,* 78–99.

Singh, P. K., Singh, V. K., Rajak, P. K., Singh, M. P., Naik, A. S., Raju, S. V., et al. (2016b). Eocene lignites from Cambay basin, Western India: An excellent source of hydrocarbon. *Geoscience Frontiers, 7*(5), 811–819.

Singh, P. K., Singh, M. P., & Singh, A. K. (2010). Petro-chemical characterization and evolution of Vastan Lignite, Gujarat. *India. International Journal of Coal Geology, 82*(1–2), 1–16.

Singh, P. K., Singh, M. P., Singh, A. K., Arora, M., & Naik, A. S. (2013). Prediction of liquefaction behavior of East Kalimantan coals of Indonesia: An appraisal through petrography of selected coal samples. *Energy Sources Part A: Recovery, Utilization, and Environmental Effects, Taylor & Francis, 35,* 1728–1740.

Singh, V. P., Singh, B. D., Singh, A., Singh, M. P., Mathews, R. P., Dutta, S., et al. (2017c). Depositional palaeoenvironment and economic potential of Khadsaliya lignite deposits (Saurashtra Basin), western India: Based on petrographic, palynofacies and geochemical characteristics. *International Journal of Coal Geology, 171,* 223–242.

Stock, A. T., Littke, R., Lucke, A., Zieger, L., & Thielemann, T. (2016). Miocene depositional environment and climate in western Europe: The lignite deposits of the Lower Rhine Basin, Germany. *International Journal of Coal Geology, 157,* 2–18.

Sun, T., Wang, C., Duan, Y., Li, Y., & Hu, B. (2014). The organic geochemistry of the Eocene Oligocene black shales from the Lunpola Basin, central Tibet. *Journal of Asian Earth Sciences, 79,* 468–476.

Suttner, L. J., & Dutta, P. K. (1986). Alluvial sandstone composition and palaeoclimate. I. Framework mineralogy. *Journal of Sedimentary Research, 56*(3), 329–345.

Sykorova, I., Pickel, W., Christanis, K., Wolt, M., Taylor, G. H., & Flores, D. (2005). Classification of huminite-ICCP system 1994. *International Journal of Coal Geology, 62,* 85–106.

Taylor, G. H., Teichmüller, M., Davis, A., Diessel, C. F. K., Littke, R., & Robert, P. (1998). *Organic petrology.* Berlin: Borntraeger.

Teichmüller, M. (1974). Generation of petroleum-like substances in coal seams as seen under the microscope. In B. Tissot & F. Bienner (Eds.), *Advances in organic geochemistry 1973* (pp. 321–348). Paris: Editions Technip.

Thomas, L. (2002). *Coal geology* (p. 89). Chichester: Wiley.

Tripathi, S. K. M., Kumar, M., & Srivastava, D. (2009). Palynology of lower palaeogene (Thanetian-Ypresian) coastal deposits from the Barmer Basin (Akli Formation, Western Rajasthan, India): Palaeoenvironmental and palaeoclimatic implications. *Geologica Acta, 7*(1), 147–160.

Varma, A. K., Biswal, S., Hazra, B., Mendhe, V. A., Misra, S., Samad, S. K., et al. (2015a). Petrographic characteristics and methane sorption dynamics of coal and shaly-coal samples from Ib Valley Basin, Odisha, India. *International Journal of Coal Geology, 141,* 51–62.

Varma, A. K., Hazra, B., Chinara, I., Mendhe, V. A., & Dayal, A. M. (2015b). Assessment of organic richness and hydrocarbon generation potential of Raniganj basin shales, West Bengal, India. *Marine and Petroleum Geology, 59,* 480–490.

Wang, S. H., & Griffiths, P. R. (1985). Resolution enhancement of diffuse reflectance ir spectra of coals by Fourier self-deconvolution: 1. CH stretching and bending modes. *Fuel, 64*(2), 229–236.

Xu, S. C., Liub, Z. J., Zhang, P., Boak, J. M., Liu, R., & Meng, Q. T. (2016). Characterization of depositional conditions for lacustrine oil shales in the Eocene Jijuntun Formation, Fushun Basin, NE China. *International Journal of Coal Geology, 167,* 10–30.